CHARACTERIZATION OF THE *cis-syn* THYMINE DIMER LESION IN DUPLEX DNA WITH NUCLEAR MAGNETIC RESONANCE

By

Belinda B. Wenke

A thesis presented to the faculty of Mount Holyoke College in partial fulfillment of the requirements for the degree of Bachelor of Arts with Honors

Department of Chemistry
Mount Holyoke College
South Hadley, Massachusetts
May, 2011

This thesis was prepared under

the direction of Dr. Megan E. Núñez

for eight credits of independent study.

ACKNOWLEDGEMENTS

I owe my deepest gratitude to my research advisor, Professor Megan Núñez for her endless patience, guidance, and encouragement. She has supported me in every facet of being a human being in academia, and I am truly grateful for the year of challenge she has offered me. I also extend my gratitude to Professors Darren Hamilton and Craig Woodard, for serving as members of this thesis committee. Thank you for all your guidance and contribution, and for being outstanding mentors. Thanks to the folks of the Mount Holyoke College Chemistry Department, who have contributed in innumerable ways by shaping my understanding and appreciation of science.

I am infinitely grateful to the sage assistance in the nuclear magnetic resonance studies from Dr. Charles Dickinson, who has worked with truly impressive patience on optimizing the parameters for these experiments. His appreciation for NMR is both remarkable and transcendent; I can only hope to one day be as capable. I would also like to thank my fellow students in the Núñez research group for their emotional support and camaraderie, and for a truly excellent summer of friendship I will never forget.

I would also like to extend thanks to my family, for their unconditional love and strangely persistent interest in my project, especially to Michael, from whom I would someday appreciate a job. I extend a final thank you to my favorite people in the world: Ivica, Dan, Seong, Alyce, Mackenzie, and all my sisters on the MHC Equestrian Team.

TABLE OF CONTENTS

List of Figures and Tables……..v

1. Abstract……vii

2. Introduction……1

2.1. DNA Damage and the Thymine Dimer Lesion…….....1
2.2. Structure and Effect of the *cis-syn* Thymine Dimer……11
2.3. Thymine Dimer Repair……14
2.4. Activation of Repair Mechanisms and Base Pair Opening…….16
2.5. Nuclear Magnetic Resonance Techniques:……19
1D and 2D NOESY
2.6. Exchange Experiments……25

3. Materials and Methods……...28

3.1. Buffer Preparation……...……..28
3.2. Sample Preparation…….…..28
3.3. NMR Sample Parameters…….……..…..30
3.4. NMR Instrument Parameters…….…..32

4. Results…….…....35

4.1. Experimental Sequences ……....35
4.2. NMR Resonance Assignment…….……..36
4.3. One-Dimensional Spectra…….....40
4.4. Two-Dimensional NOESY Spectra……..44
4.5. Assigned One-Dimensional Spectra…….....52
4.6. Exchange Experiments…….62

5. Discussion……82

5.1. Sequence Selection……82
5.2. NMR Resonance Assignment: Duplexes KK56 and KK5TT6….83
5.3. NMR Resonance Assignment: Duplexes KK34 and KK3TT4..85
5.4. Exchange Experiments…….89
5.5. Relation to Homologous Research……93

6. Conclusion…….…96

7. References…….……97

LIST OF FIGURES

Figure 1. Canonical Watson-Crick base pairing of the four nitrogenous bases 4

Figure 2. The structure of a cyclobutane pyrimidine dimer (CPD) formation induced by UV-C radiation 7

Figure 3. The multiple valence isomers of the cyclobutane pyrimidine dimer photoproduct 10

Figure 4. A crystal structure of the *cis-syn* thymine dimer lesion incorporated into a duplex of DNA 13

Figure 5. A schematic of the interior of an NMR Spectrometer 20

Figure 6. A sample 2D NOESY assignment, from a simple DNA sequence of 5'- G G A -3' 23

Figure 7. Sample 2D NOESY proton spectrum 24

Figure 8. Sample diagram of a trimer 5'- A G C -3' 39

Figure 9.1D spectrum of KK34 41

Figure 10. Imino region of KK34, with no assignment 43

Figure 11. Expanded imino proton region (12-14 ppm) of 2D NOESY spectrum of KK56 45

Figure 12. Expanded imino proton region (12-14 ppm) of 2D NOESY spectrum of KK5TT6 47

Figure 13. Expanded imino proton region (12-14 ppm) of 2D NOESY spectrum of KK34 49

Figure 14. Expanded imino proton region (12-14 ppm) of 2D NOESY spectrum of KK3TT4 51

Figure 15. 1D spectrum of imino proton region (12-14 ppm) of the parent strand KK56 53

Figure 16. 1D spectrum of imino proton region (12-14 ppm) of the dimer strand KK5TT6 56

Figure 17. 1D spectrum of imino proton region (12-14 ppm) 59

of the parent strand KK34

Figure 18. 1D spectrum of the expanded imino proton region (12-14 ppm) of KK3TT4 61

Figure 19. Water inversion and recovery 63

Figure 20. KK34 parent imino proton spectra as a function of mixing time, in 40 mM ammonia catalyst 65

Figure 21. KK3TT4 dimer imino proton spectra as a function of mixing time, in 40 mM ammonia catalyst 67

Figure 22. Individual imino protons of KK34 in 40 mM ammonia catalyst 69

Figure 23. Individual imino protons of KK3TT4 in 40 mM ammonia catalyst 71

Figure 24. Overlaid imino regions of KK34 for five increasing catalyst concentrations 73

Figure 25. KK3TT4 imino region at four increasing ammonia catalyst concentrations of 40, 80, 120 and 200 mM 75

Figure 26. Exchange rates for each residue plotted against ammonia concentration 78

Figure 27. Plot of KK3TT4 exchange rate per residue as a function of ammonia catalyst concentration for four concentrations 80

Figure 28. Chemical shift changes in the KK34 to KK3TT4 duplex 87

LIST OF TABLES

Table 1. Extinction coefficients. 30

Table 2. Experimental process and mixing time. 34

Table 3. Sequence of 12-mer DNA Oligonucleotide Duplexes. 35

Table 4. Sequence of 10-mer DNA Oligonucleotide Duplexes, from Taylor *et al.* 36

Table 5. Chemical shifts (in ppm) of imino proton resonances in the parent (KK56) complex versus dimer complex (KK5TT6). 57

Table 6. Chemical shifts (in ppm) of imino proton resonances in the parent (KK34) complex versus dimer complex (KK3TT4). 62

Table 7. Exchange rates and base pair lifetimes. 77

Table 8. Values for equilibrium constant of opening for each residue. 81

1. ABSTRACT

Ultraviolet irradiation from sun exposure can lead to permanent, covalent damage in DNA. The damaged sites can block the progression of polymerases, thereby preventing replication or transcription. The frequent occurrence of lesions in the genome necessitates rapid and effective internal repair mechanisms, as well as a highly sensitive detection mechanism to initiate repair. Perturbations in the three-dimensional solution-state structure of the DNA duplex may alert repair proteins to a damage site. Our experiments model the occurrence of a *cis-syn* thymine cyclobutane dimer lesion, hereafter called the thymine dimer, which results as the major photoproduct of UV irradiation of two adjacent thymines. The two bases form a cyclobutane ring *via* a [2+2] cycloaddition. The thymine dimer has been considered a bulky and destabilizing lesion; published structures of the thymine dimer lesion reveal that the backbone around the lesion is pinched, the DNA is kinked, and the canonical Watson Crick base pairing with the opposite adenines is disrupted through the loss of one hydrogen bond, weakening the interactions with the complementary strand. We hypothesize that the hydrogen bond disruption from the formation of the lesion results in an increased rate of imino proton exchange from the affected thymine bases. We further predict that an increased rate of proton exchange would correlate to an increased rate at which the bases spontaneously flip out of the double helix conformation, alerting repair enzymes to a damage site.

Two-dimensional NMR was used to characterize the imino region of a 10-mer and 12-mer undamaged parent complexes and dimer-containing lesion complexes. Assignment of resonances to specific exchangeable base protons was accomplished through sequential connection of Nuclear Overhauser Effect (NOE) cross-peaks, which result from through-space (rather than through-bond) interactions between protons that are less than ~ 6Å apart.

In comparing the imino region of the parent and dimer 12-mer duplex spectra, we observed that the thymines associated with the dimer (T6 and T7) exhibit noticeable upfield shifts in resonance frequency. The thymine at the 5' end of the dimer (T6) is isolated and does not overlap with neighboring peaks. However, in both the parent and dimer sequences, the thymine residue on the 3' side of the lesion, T7, is overlaid with a second peak. In the parent, thymines 7 and 9 overlap, and in the dimer, thymine 7 and guanine 14 are overlaid. The position of T7 is not ideal, especially compared with the clarity of T6. Since T7 overlaps with other peaks, we cannot accurately observe changes in behavior once the dimer is introduced. In the 10-mer duplex, a similar upfield shifting effect was observed, but every residue (including dimer residues T5 and T6) is well resolved in both parent and dimer structures. Thus, the 10-mer sequence was used to measure quantitatively the kinetic destabilization using imino exchange experiments.

From the exchange experiments, the 5' thymine dimer residue T5 had an equilibrium constant of opening of $0.11 \times 10^{-6}\ M^{-1}s^{-1}$ in the parent complex, and increased more than tenfold to $1.4 \times 10^{-6}\ M^{-1}s^{-1}$ in the dimer form.

Significant increases in equilibrium constants of opening were also observed for the flanking thymine residues T14 and T17, with a modest increase in T6. The increase in equilibrium opening constant for T5 indicates that there is a kinetic effect of the dimer that allows rapid, frequent exchange of the imino proton. Our data support the suggestion that the *cis-syn* cyclobutane thymine dimer destabilizes the DNA duplex enough to augment base opening to the solvent significantly.

2. INTRODUCTION

2.1. DNA Damage and the Thymine Dimer Lesion

Deoxyribonucleic acid (DNA) is the fundamental genetic material in modern organisms. Genetic material is iteratively copied to generate successive generations, and stability of the genome is essential in preventing degradation of the genetic information with each successive inheritance. Considering that efficient, accurate replication of DNA is critical to the success of every organism, researchers initially incorrectly assumed that DNA was infrequently exposed to or easily able to resist chemical modification. (*1*) The stability of DNA is not actually a result of resistance to modification, but in large part to the ability of the complex DNA repair networks to edit and restore genetic material. DNA is under constant attack by both endogenous and exogenous sources. Endogenous sources include hydrolytic and oxidative damage that occur from the hostile cellular environment, which is aqueous and constantly infiltrated by reactive oxygen byproducts from metabolism. (*2*) Exogenous sources are generated outside the cell, and include physical and chemical agents that damage DNA. The accumulation of damage can lead to mutations in the DNA sequence, ultimately causing uninhibited cellular proliferation (cancer), cellular senescence (aging), or cellular apoptosis (death). Thus, it is necessary to understand the formation and consequences of DNA damage.

DNA is a polymer made of monomeric units composed of nitrogenous bases and ribose sugars, connected by phosphodiester linkages. The DNA molecule is prone to damage at any site, but damage to the nitrogenous bases is of particular interest, since the bases code for the genetic material. Four nitrogenous bases compose normal DNA structure: adenine, thymine, cytosine and guanine (Figure 1). The bases are stabilized within a DNA double helix superstructure through hydrogen bonding to their canonical Watson-Crick base pair. The strands of the helix are oriented in an anti-parallel fashion, with the bases flat in a plane perpendicular to the sugar-phosphate backbone. Polymerization of each stand is continued by bonding a 5' carbon phosphate group of one nucleotide to the 3' carbon hydroxyl group of a second nucleotide through a phosphodiester linkage. The strand orientation is thus described by "5' to 3'", which describes the orientation of the non-bonded 5' or 3' carbon end. Stability of the duplex structure derives from both the hydrogen bonding complementarity of the nitrogenous bases, and the van der Waals stacking interactions of the hydrophobic bases. The aromaticity of the bases could allow π electrons to freely diffuse along the central axis of the helix, but this theory is controversial and remains an area of dispute in the field.

The conformation of the DNA duplex can adopt multiple forms. The structure elucidated by Watson and Crick is of B-form DNA, which is characterized by a wide major groove and narrow minor groove, and right-handed helical turns. B-DNA contains a 3.4 nm helical repeat distance, and a

0.34 nm distance between two neighboring bases, such that 10 base pairs complete one turn (*3*). A-form DNA is a right-handed helix form that occurs in high salt concentrations, i.e. those larger than physiological salt concentration of 0.15 M KCl, 0.004 M $MgCl_2$ (*4*). A-DNA also has a helical pitch of 2.3 nm with 11 base pairs per turn, and the differences in the major and minor groove are less distinct, due to the lengthening along the central axis of the overall duplex. Z-DNA is a left-handed form, with a helical pitch of 4.6 nm or 12 base pairs per turn. Z-DNA often forms at sites of transcription, where duplex DNA is unwound to accommodate replicating polymerases, and also at particular G•C alternating sites in high salt concentrations (*5*).

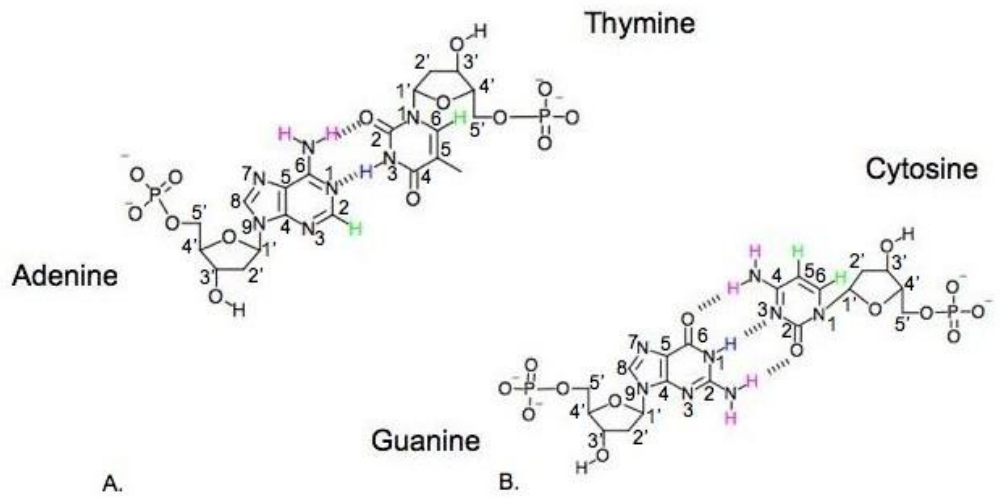

Figure 1. Canonical Watson-Crick base pairing of the four nitrogenous bases: (A.) An adenine/thymine base pairing. (B.) A guanine/cytosine pair. Hatched lines indicate the region of hydrogen bonding, where a C-G pair has three hydrogen bonds, and an A-T pair has two. Standard numbering of the ribose and base ring is shown. Important protons on the bases are highlighted: amino protons are in purple, imino protons are in blue, and aromatic ring protons are in green.

Multiple forms of exogenous DNA damage can occur spontaneously. For example, adenine, guanine and cytosine contain amine groups that can be spontaneously cleaved from the base at physiological pH (7.5) and temperature (37°C) (*2*). The deamination can result in mismatched pairing during the replication process, since the amine group is critical in the normal hydrogen bonding (Figure 1). Similarly, bases can be spontaneously cleaved out of the duplex at the N-glycosyl bond, leaving an abasic site and exposing the phosphodiester backbone to ester hydrolysis. The mechanism of hydrolysis follows a sequence of protonation of the base, then direct cleavage of the N-glycosyl bond. Both purines and pyrimidines can be lost from the duplex at significant rates in acidic pH by acid catalysis. Cleavage of the backbone can result in single-strand breaks (nicks), or full double stranded breaks, which can lead to severe heritable mutations (*2*).

Oxidative DNA damage is more common than spontaneous hydrolysis. Reactive oxygen species are continuously produced as a by-product of aerobic metabolism during which oxygen becomes the final electron acceptor. Molecular oxygen (O_2) is relatively unreactive towards DNA, but unpaired orbitals can accept single electrons to create radical oxygen ($\bullet O_2^-$). Radical dioxygen itself is not very reactive to DNA, but it can easily form superoxide (H_2O_2), which can decompose to generate hydroxyl radicals ($\bullet OH$). Multiple processes such as release of antioxidants and degradative enzymes help control the population of reactive oxygen species, but often the redox equilibrium is upset by exposure to radiation and redox-

active chemicals (*2*). Oxygen radicals can perform a variety of reactions on DNA bases in particular; hydroxyl radicals can abstract hydrogen atoms from the sugar rings or add across double bonds in the DNA bases. A common lesion resulting from oxygen free radicals is 7,8-dihydro-8-oxoguanine, a mutation of guanine with an oxidized imidazole ring. The oxidation of guanine causes the base to more readily adopt the *syn* conformation, which can mismatch through the formation of hydrogen bonds with adenine. The mismatch often leads to errors in replication (*6*).

A classic system in which to study DNA base lesions is the irradiation of cells with ultraviolet (UV) light. Studies of UV light effects are of particular biological relevance, because organisms must contend with constant solar UV radiation. UV light is subdivided by wavelength into UV-A (320 to 400 nm), UV-B (295-320 nm) and UV-C (100-295 nm). The atmospheric ozone layer only allows penetration of mainly UV-A and UV-B, but frequently, UV-C light is used to induce DNA damage *in vitro*. DNA absorbs at 260 nm, unlike most proteins, and is thus efficiently and specifically excited by UV-C irradiation (*2*). Ultraviolet light irradiation induces multiple kinds of DNA damage, most commonly cyclobutane pyrimidine dimers. A lesion results as the major photoproduct of light-promoted [2+2] cycloaddition of two adjacent pyrimidine bases, in a Diels-Alder –like reaction (Figure 2).

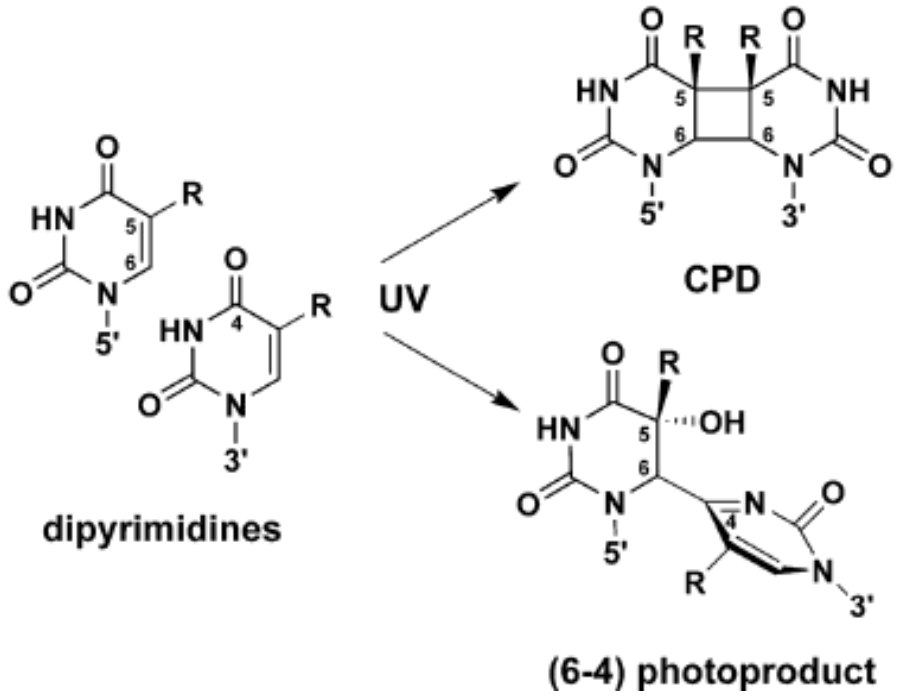

Figure 2. The structure of a cyclobutane pyrimidine dimer (CPD) formation induced by UV-C radiation. The minor 6-4 photoproduct is also shown. Taken from Li *et al.*, 2006. (*7*)

Adjacent pyrimidines become covalently bonded by cyclobutane ring formation between the carbon 5 and 6 positions, destabilizing the bases through loss of aromaticity. Cyclobutane ring formation can yield several isomeric conformers: *cis-syn*, *cis-anti*, *trans-syn*, or *trans-anti*. (Figure 3) The variability of the structural isomers is dependent on the orientation of the nitrogenous base to the sugar ring, as well as the position of the nitrogenous bases relative to each other. The *cis-trans* conformation of the CPD occurs from the variation of the position of the base relative to the ring, and the *syn-anti* conformation is dependent on whether the C5-C6 bond of each base are parallel to each other, or anti-parallel, respectively (*8*).

Most commonly in regular B-form DNA, adjacent thymines are susceptible to dimerization in the *cis-syn* orientation in which the C5-C6 bonds are parallel and the thymine is in the *cis* conformation to the ribose ring. The *cis-syn* thymine dimer is often abbreviated T<>T. The *trans-syn* dimer can be more commonly formed in partially denatured DNA, where the bases have more freedom of conformation. In regions of active transcription where the duplex DNA is often unwound to accommodate polymerases, cyclobutane pyrimidine dimers can occur between nonadjacent pyrimidines (*2*).

In naturally occurring genomes, dimerization between thymines occurs more frequently than dimerization between two cytosines or between a thymine and a cytosine. The ratio of thymine-thymine dimers (T<>T) to cytosine-thymine dimers (C<>T) to thymine-cytosine dimers (T<>C) to

cytosine-cytosine dimers (C<>C) is 68:13:16:3 in human cells irradiated with UV-B radiation at 254 nm (*9*). The occurrence of thymine dimer lesions reaches photochemical equilibrium once 7% of the thymines in the sequence have been converted to dimers (*10*). At photochemical equilibrium, the rate of dimer formation and dimer dissociation are equal. Dimer formation can be reversed by photo-reversal, when a sufficiently high dose of UV radiation can break the covalent bonds of the cyclobutane dimer.

In almost all other contexts, the thymine dimer is a very stable structure. The lesion is resistant to extremes of pH as well as temperature. Complete acid hydrolysis of the DNA superstructure will yield thymine dimer units that can be separated from the remaining nucleic acids (*2*).

Many characteristics of the thermodynamic properties of the thymine dimer lesion are known. Duplex formation of two single stranded oligonucleotides, one containing a thymine dimer lesion, occurs readily at room temperature with a large negative Gibbs free energy. Compared to the Gibbs free energy of duplex formation of non-damaged strands, the change in free energy is very low, suggesting the dimer has a low level of thermodynamic effect. Although previous studies have suggested that the destabilization is an entropic effect, the opposite thermodynamic effect is observed in samples with other oligonucleotide lengths and sequences (*11*).

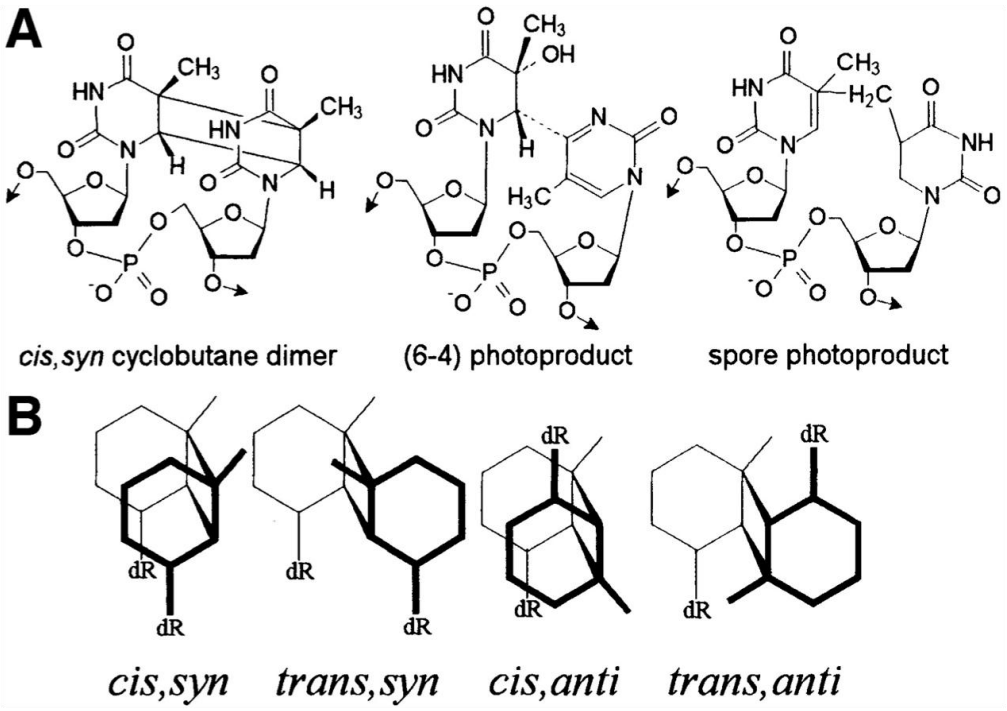

Figure 3. The multiple valence isomers of the cyclobutane pyrimidine dimer photoproduct. The *cis-trans* conformation is dependent on the position of the base relative to the ring, and the *syn-anti* conformation is dependent on the parallel or anti-parallel orientation of the C5-C6 bonds. Taken from Douki *et al.*, 2003. (*8*)

2.2. Structure and Effect of the **cis-syn** *Thymine Dimer*

Cyclobutane pyrimidine dimers have classically been considered as bulky and helix-distorting. The thymine dimer lesion is known to have destabilizing effects on the DNA superstructure by creating a pinching effect in the phosphodiester backbone and kinking the regular B-DNA form. The presence of the lesion weakens interactions with the complementary strand through loss of one hydrogen bond with the opposite adenines (*12*). CPDs were assumed to be unconditionally non-coding lesions, causing a discontinuation in the activity of RNA polymerases to transcribe the DNA. In the *cis-syn* thymine dimer, disruption is based on the chemical structure of the lesion, in which the hydrogen bonding to the opposite strand is affected. The distortion in the helix structure can create a bubble of single-stranded DNA, causing polymerases to pause (*2*).

In some instances, the thymine dimer lesion causes disruptions by blocking the progression of DNA and RNA polymerases, but polymerases in the error-prone Y super family can bypass a variety of CPD lesions, by virtue of large, accommodating active sites (*2*). *In vivo*, the lesion can be eliminated or repaired by transcription-coupled repair (TCR) and nucleotide excision repair (NER) pathways in eukaryotes, or by photoreversal through continued UV radiation. In TCR, the first step of repair is when RNA polymerase pauses at the lesion site. (*13*)

Although the presence of the lesion is described as highly destabilizing, the *cis-syn* thymine dimer lesion can be effectively incorporated

into B-DNA double helix structure, and maintain some hydrogen bonding to the opposite strand (*2*). X-ray crystallographic methods have previously been used to characterize the lesion within an overall helix, and comparisons to regular B-form DNA indicate little overall disruption, only local distortion within the helix (*14*). The fused ring structure participates in normal base stacking, which is the primary source of DNA duplex stability. Quantitative distortions within the helix are disputed, but X-ray crystallographic methods from Park *et al.* show that the *cis-syn* thymine dimer creates a 30° bend in the DNA towards the major groove, introducing a region of widened minor grove. The bend angle is in contrast to previous NMR studies by Kim *et al.* that report a 9° bend towards the major groove. (*15*) However, the data from Park *et al.* is consistent with prediction of a 27° bend from mathematical modeling. (*14*)

In other observations, there is a consensus. From the crystal structure from Park *et al*., (Figure 4) the minor groove is pinched proximal to the 3' side of the thymine dimer lesion, but long-range effects show the major and minor groves are widened 3' and 5' of the lesion for the whole duplex. The DNA is unwound 9°, in agreement with early structural estimates. The crystal structures showed only minor deviations from regular B-form DNA, which indicates that the overall DNA helix accepts the strain at the lesion site by conformational stress immediately near the lesion, instead of distributing the distortion throughout the duplex.

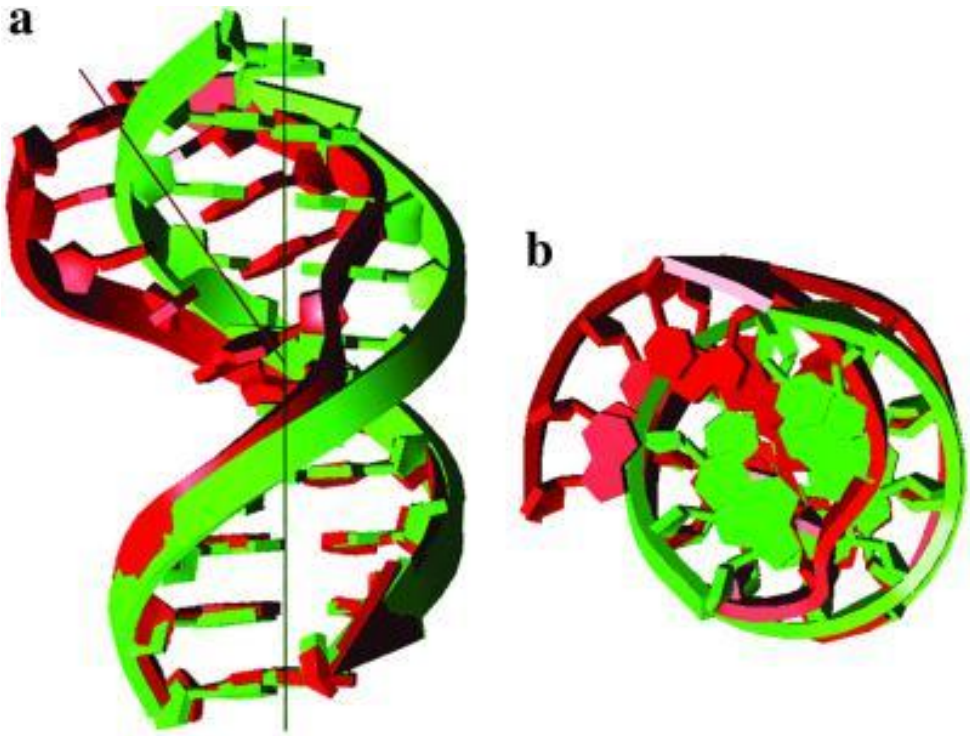

Figure 4. A crystal structure of the *cis-syn* thymine dimer lesion incorporated into a duplex of DNA. Regular B-DNA is shown in green, and the thymine-dimer containing duplex is shown in red. (A) Side view of the helical axis, with 30° bend towards the major groove, away from the helical axis, is indicated. (B) Top view of the duplex. Taken from Park *et al*., 2002. (*15*)

2.3 Thymine Dimer Repair

Lesion repair and removal necessitates activation of repair enzymes, and although the distortions to the overall helix are not catastrophically disturbing, the lesion site must be significantly different from regular B-form DNA to trigger repair. The *cis-syn* thymine dimer can be repaired by enzymatic photoreactivation in prokaryotes, or by nucleotide excision repair (NER) in eukaryotes. (*2*)

Photolyases are a class of enzymes that can transduce external light for catalytic purposes. Photoproduct-DNA (PD-DNA) photolyases exist in class I and class II forms, identified only in prokaryotes and fungi. PD-DNA photolyases contain two non-covalently bound chromophore moieties that absorb environmental light of specific wavelengths (*2*). The photolyases can absorb visible light and perform catalysis in a two-step process. The association of the enzyme to the DNA duplex containing the CPD is referred to as the "dark reaction", and the dissociation of the enzyme from a repaired DNA duplex is the "light reaction". In the "dark reaction" activity is performed without light of wavelengths 300 and 500 nm (photoreactivation wavelengths). *E. coli* PD-DNA photolyase can bind to the DNA duplex in a specific manner, at about 2×10^5 M^{-1} (*16*). The relative specificity of the binding suggests that the photolyase can target the site of CPD lesion, instead of randomly binding other thymine bases. In the "light reaction", a chromophore transfers a blue-light photon to a flavin cofactor, which donates the electron to the dimer lesion, breaking the cyclobutane ring. (*16*)

In eukaryotes, CPDs and other lesions resulting from UV-light damage are repaired through nucleotide excision repair (NER). The purpose of NER is to remove particularly bulky and helix-distorting lesions, as opposed to the more specific base excision repair (BER) pathway. In BER, enzymes can locate and excise individual bases, breaking the N-glycosyl bond between the base and the sugar, allowing polymerases to fill the site. In NER, a brief single-stranded DNA region is removed altogether.

In *E. coli*, the UvrABC endonuclease enzyme complex controls the NER pathway. The *E. coli* system is well characterized, consisting of the Uvr family of proteins: UvrA, UvrB, UvrC, and DNA helicase II, or UvrD. The NER mechanism works through initial scanning of the genome by a Uvr-A, UvrB complex. The UvrA subunit can detect distortions in the helix, such as those created by CPDs. Upon recognition of a lesion site, UvrA dissociates from the complex, and is replaced by UvrC, which dimerizes with UvrB. A 12-base pair long stretch of DNA is cleaved by the UvrB-UvrC complex; UvrB creates a single-strand break four bases to the 3' of the lesion site, and UvrC breaks the phosphodiester backbone eight bases to the 5' side of the lesion. The action of removing the single-stranded oligonucleotide is completed by DNA helicase II, which breaks the Watson-Crick hydrogen bonds between the strands. The unaffected single-stranded DNA can be used as a template for fresh synthesis by DNA polymerase I and DNA ligase (*5*).

The NER pathway in eukaryotes contains greater complexity than the well-studied cascade in *E. coli.* The protein cascade is less well known for

higher eukaryotes, but the proteins involved in the *E. coli* system are homologous to those in eukaryotes. Compared to *E. coli*, a large segment of 25-30 nucleotides are excised and replaced by DNA polymerase δ or ε (*5*).

2.4 Activation of Repair Mechanisms and Base Pair Opening

The cascade of protein recruitment has been well studied, but the exact mechanism of initial enzyme recruitment to the lesion site is still debated. As previously stated, the specificity of an enzyme complex to a lesion site suggests that the repair enzymes are somehow alerted and summoned to the damaged site, by a very sensitive mechanism.

A mechanism of repair enzyme activation may be dependent on a kinetic signal. The dynamic motions of DNA in solution could be useful to enzymes in detecting minor perturbations in normal motion of the duplex structure. There are many forms of DNA motion: DNA bending occurs on a slow timescale, whereas vibrations on the bases occur very fast (on the order of picoseconds). Kinetic movements of DNA include spontaneous base opening. In solution, bases within a helix structure are dynamic, and bases can flip out to face the solvent using the glycosidic bond as a hinge. Base pair opening is classified as a two-state model, characterized by an open state in which the imino proton of guanine or thymine can exchange with the solvent, and a closed state in which no exchange occurs due to involvement of the imino proton in hydrogen bonding (*17*). The two state model is limited as it is not known when imino exchange occurs during the flipping event. The open

base has a lifetime on the order of nanoseconds and capturing the exact moment of proton dissociation is difficult. Exchange could occur from flipping out the base containing the imino proton (guanine or thymine), or it could occur from opening its Watson-Crick pair (cytosine or adenine). The known value for a G•C base pair lifetime is approximately 10-50 ms, and the corresponding lifetime for an A•T base pair is 1-5 ms. Similarly, the equilibrium constant for open and closed states is known to be on the order of $10^{-6} – 10^{-7}$ (*17*).

However, the model of base pair opening can be useful in determining the rate constant for opening and closing, as based on experiments suggested by Guéron and Leory. The theory of imino exchange experiments is based on the exchange of a proton between an imino proton bonded to a nucleotide (Nuc) and a proton acceptor (acc): (*18*)

$$\text{NucH} + \text{acc} \Leftrightarrow \text{NucH}--\text{acc} \Leftrightarrow \text{Nuc}--\text{acc}^{+}\text{H} \Leftrightarrow \text{Nuc}^{-} + \text{acc}^{+}\text{H} \qquad (1)$$

The first step is the complex formation, the second is the proton transfer (with a rate k_{tr}), and the third step is dissociation, leading to the final step of completed transfer (with a rate k_{ex}). To complete the assumption of the system, the pH of the solution must be smaller than the pK_a of the nucleotide, so that most nucleosides in solution are protonated and available for exchange. In this case, the rate-limiting step is nucleoside deprotonation. Similarly, the experiments also assume that the rate of proton exchange (k_{ex}) is equal to the rate of transfer from nucleoside to acceptor (k_{tr}). The rate of transfer (k_{tr}) is defined, according to standard collision theory, as the product of the fraction

of productive dissociations leading to transfer (F) and the rate of complex formation, which is defined as the rate constant of collision (k_{coll}) and the concentration of acceptor:

$$k_{tr} = F*k_{coll}*[acc] \quad (2)$$

The fraction of productive collisions is related to the pK_a's of the donor and acceptor. The system parameters allow exchange time (τ) to be defined as

$$k_{tr} \equiv 1/\tau_i = k_{coll}[acc] /(1 + 10^{pK(nuc)-pK(acc)}) \quad (3)$$

in which τ_i refers explicitly to the exchange lifetime of a nucleotide free in solution.

Within the double helix structure, the complexity increases, because exchange is also dependent on the rate of base pair opening since exchange cannot occur without an opening event. Exchange lifetime for a base in a duplex (τ_{ex}) is defined as the sum of:

$$\tau_{ex}= \tau_0 + \tau_i(1 + 1/K_{diss})/\alpha \quad (4)$$

The exchange time (τ_{ex}), is dependent on base pair lifetime (τ_0), with several corrections for the dissociation of the proton and involvement of the active catalyst (included in a constant, α). (*18*)

With a sufficiently high catalyst concentration, exchange can occur for each opening event, in which case the exchange time can be called the base-pair lifetime. Exchange times have been found to be strongly dependent on the concentration of an exchange catalyst. Extrapolating to infinite catalyst concentration models an exchange event occurring with every opening (*19).*

In our experiments, the exchange rate (k_{ex}) is experimentally determined, and from exchange rate (k_{ex}), we take the inverse to find base pair lifetime (τ_0).

2.5 Nuclear Magnetic Resonance Techniques: 1D and 2D NOESY

Nuclear magnetic resonance spectroscopy (NMR) uses the magnetic properties of nuclei to determine physical and chemical properties, including information about the structure and dynamics of molecules. Every nucleus has a specific resonance frequency depending on chemical environment, and from this principle, structure can be characterized. Additionally, exchange experiments can yield exchange rates through measuring the intensity of any exchangeable peak as a function of mixing time.

The NMR instrument consists of three main components: a coil of superconducting wire to create a strong magnetic field, a probe that can send and receive radio-frequency signals, and a computer that can convert radio-frequency signal that can be interpreted to yield information of chemical environment. Within the core of the NMR, a strong magnetic field is produced in the Z-direction (Figure 5). Nuclei with a dipole moment will align themselves according to the magnetic field (B_0) at equilibrium. Radio-frequency signals, or pulses, are delivered to the sample in the X-Y plane, perpendicular to the Z-axis, causing the nuclei to orient their magnetic moments in that direction. As the nuclei return to equilibrium, radio frequency signals are emitted, which can be Fourier-transformed into readable peaks.

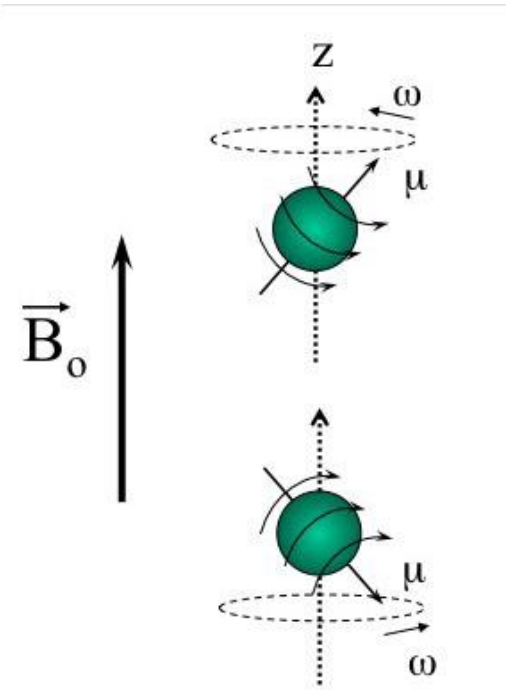

A.

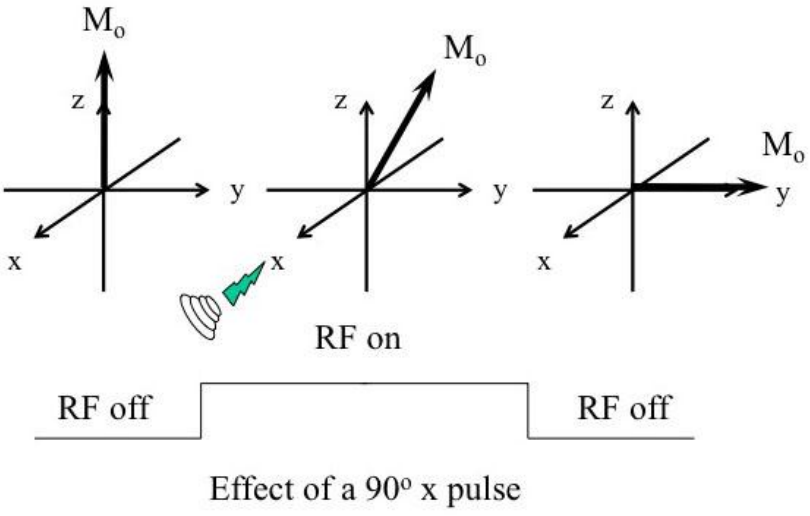

B.

Figure 5. (A) A schematic of the interior of an NMR spectrometer. The applied magnetic field B_0 is shown, oriented in the Z direction. The nuclei are shown to have a dipole moment (μ), and a Larmour frequency (ω). (B) A simple 90° pulse. Taken from Bishop, 2011. (*20*)

The DNA duplex structure can be elucidated through two-dimensional NMR methods that take advantage of the overlaps in radio-frequency emissions of neighboring nuclei in space. The simple one-dimensional NMR experiment yields a spectrum with intensity on the Y-axis and frequency on the X-axis. The sample is pulsed, and the data are collected over a mixing time to yield the spectrum. In two-dimensional NMR, there are two mixing times at which data is collected. In this case, the spectra are reported with two frequency axes, corresponding to the two peak intensities found as a function of two mixing times.

A common 2D method for structure characterization is Nuclear Overhauser Effect Spectroscopy (NOESY). NOESY is a technique that shows the Nuclear Overhauser Effect (NOE) interaction between nuclei, represented as a cross-peak on the spectrum (Figure 6). NOE's are observed between nuclei in a through-space (rather than scalar through-bond) interaction, as their resonances interact. Two nuclei must be less than 6Å apart to observe the effect. In Figure 6, a sample NOESY can be generated from a sequence of nucleic acids showing interactions between the ribose ring protons (H1') and the nitrogenous base protons (H6 for C and T, and H8 for A and G). The radio-frequency signals reflect these interactions that can be transformed into peaks relaying the same information. From these peaks, a "walk" connects them. The H1' proton has a 2D NOE cross-peak at a specific frequency that aligns with the frequency of an H6 or H8 aromatic ring proton of a neighbor, as well as an alignment with the H6 or H8 on its own ring. Each type of

proton has its own specific range of frequencies. The applications are diverse, since every proton can yield cross-peaks, given that it has a neighbor to interact with. An assignment of the cross-peaks in a DNA sequence involves laborious understanding of both the molecular structure of the DNA (what protons can interact with each other?), as well as the sequence (logically, which protons belonging to which residues should interact?). Assigning an NOE walk becomes challenging for large molecules because the peak density is increased, and part of the assignment includes deciphering which peaks are noise, and which peaks are relevant protons. The determination of significant peaks requires careful assignment of the residues that “see themselves”, and examining the spectrum along that resonance frequency for neighbors. In a typical NOESY spectrum (Figure 7), a strong diagonal series of peaks is observed, correlating to the internal interactions of a base. Cross-peaks off of and symmetrical along the diagonal represent the NOE interactions. The structure of a DNA duplex can be unambiguously elucidated from connecting the cross-peaks of the nuclei, through the NOE walk mentioned previously. Neighboring nuclei will share a cross-peak, and from the logical solution of the spectrum, the structure can be determined.

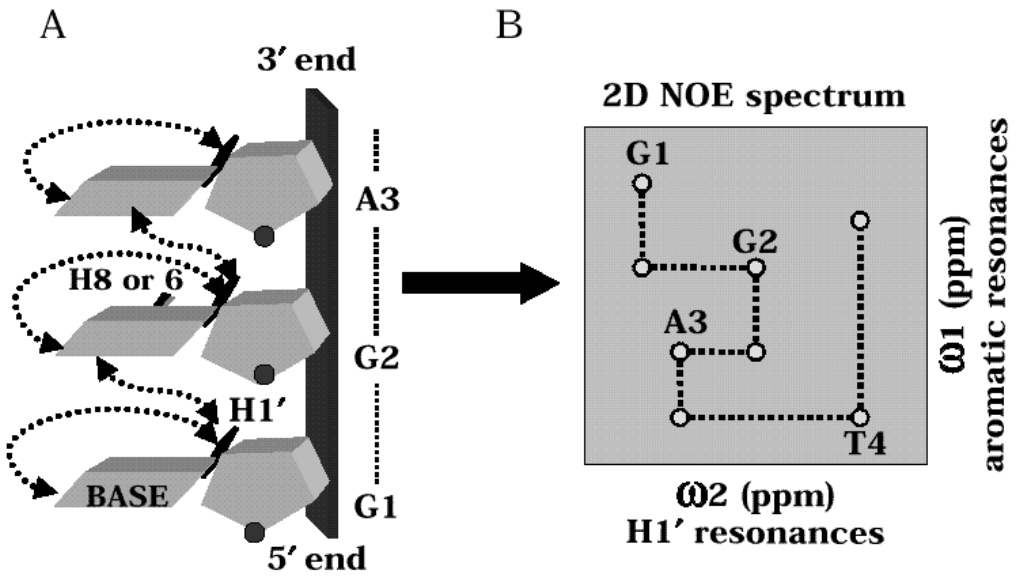

Figure 6. A sample 2D NOESY assignment, from a simple DNA sequence of 5'- G G A -3'. (A.) The dotted arrows indicate NOE interactions between the H1' proton on the ribose sugar, represented as a hexagon, and the H8 or H6 protons on the base, represented as parallelograms. (B.) The interactions are converted to peaks on a spectrum, with two frequency axes: an aromatic axis from the base, and an H1' axis from the sugar. The G1 residue shares a cross-peak with G2, through the interaction between the H1' of G1 to the H8 of G2. Similarly, the G2 residue has a cross-peak to A3, and so forth. Taken from James, 2001. (*21*)

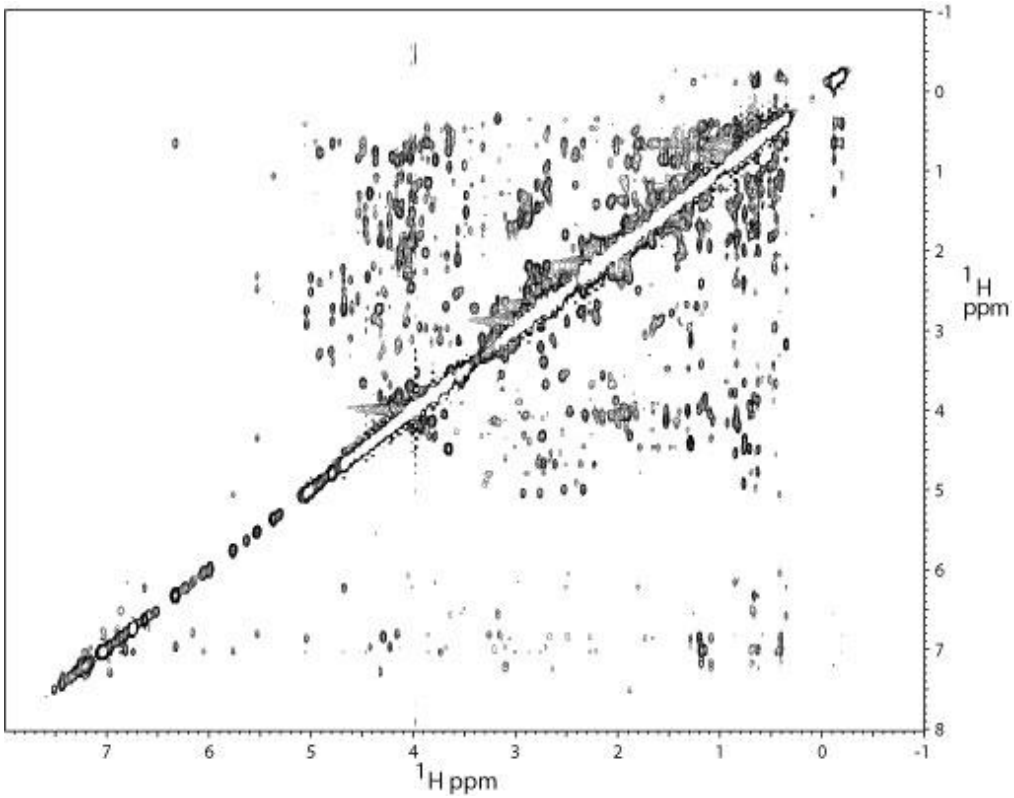

Figure 7. Sample 2D NOESY proton spectrum. The two frequency axes are noted in ppm. The strong diagonal peak is noticeable, with cross-peaks observed on either side. Taken from Fawzi *et al*., 2008. (*22*)

2.6. Exchange Experiments

To determine the opening lifetime τ (Equation 3), we will measure the exchange rate of the imino protons. In order to determine exchange rate (k_{ex}), NMR experiments can be used to magnetically label solvent protons, which exchange with imino protons on the DNA duplex. In our experiments, solvent protons are magnetically labeled by selective 180º inversion, which then undergo catalyzed exchange with imino base protons on the duplex with and without a *cis-syn* thymine dimer lesion.

Initial inversion-recovery experiments of the solvent water protons can be accomplished to determine the frequency and magnetically label the protons with precision. Relaxation rate (Rl_w) of the water protons recovering from the 180° pulse are related to the intensity of the water signal at equilibrium (W_z) as a function of mixing time (t_{mix}):

$$W(x) = W_{eq} * (1.0 - E * e^{-xRl_w}) \qquad (5)$$

The water protons and imino protons relax to equilibrium simultaneously. The exchange rate for each imino proton in the duplex can be found by fitting the peaks to the variables exchange rate (k_{ex}) and imino proton relaxation rate (Rl_i):

$$\frac{I_z(t_{mix})}{I_{z\,eq}} = 1 + Ek_{ex}\left[\frac{e^{-Rl_i t_{mix}} - e^{-Rl_w t_{mix}}}{Rl_w - Rl_i}\right] \qquad (6)$$

The intensity of the imino peaks at and off equilibrium are $I_z(t_{mix})$ and $I_{z,eq}$. Other pertinent factors include the efficiency of water inversion (E), which is ideally -2 for 100% efficiency. Exchange rate k_{ex} can be obtained for each

imino proton at multiple catalyst concentrations [B]. The rates of base pair opening and closing (k_{op} and k_{cl},) can then be found with the relationship:

$$\frac{1}{k_{ex}} = \frac{1}{k_{op}} + \frac{k_{cl}}{\alpha * k_{op} * \left([B] * k_B + k_{int}\right)} \qquad (7)$$

This equation shows that the inverse of exchange rate is related to the inverse of the rate of opening, plus a second term. The second term includes the rate of closing divided by rate of opening (which is equal to K_{op}, the equilibrium constant of opening), the correction term α (for the dissociation of the proton and involvement of the active catalyst), and a term for the catalyst concentration B, the collision rate k_B, and the rate of internal catalysis on the base. So, the inverse exchange rate is equal to the inverse rate of opening, plus the equilibrium constant of opening, with a correction factor.

A variety of base catalysts have been used in proton exchange experiments, such as ammonia, trimethylamine and glycine. Ammonia has an advantage over other catalysts in that it has an observable effect at a low concentration (milli-molar range). Catalysts that require higher concentrations can influence structural or dynamic properties of the duplex DNA, and skew the equilibrium constant for closed and open states. Ammonia at the milli-molar range has little effect on the overall duplex structure, and it has been found to increase the relaxation rates of exchangeable protons by 50% (*23*). An additional benefit is that all the ammonia protons exchange completely with the solution so that no additional ammonia peak appears in the NMR data.

The concentration of active ammonia catalyst [B] can be found by using the Henderson-Hasselbalch equation, knowing the pK_a of ammonia is 9.25 and the system pH is 7.5. Roughly 18 ammonia ions are active out of 1000, or 1 in 56.

In equation 7, k_B is a term for the molecular collision rate and the relative ability of the base to abstract the proton from the nucleoside.

$$k_B = \frac{k_D}{1+10^{pK_{a(Nuc)} - pK_{a(B)}}} \qquad (8)$$

In our data, we approximated that our catalyst concentration was still sufficiently low, and therefore the exchange rate is so slow that that the $1/k_{op}$ term is negligible thus the points can be fit to a line (*24*), where

$$k_{ex} = k[B] * K_{op} * [B] + K_{op} * K_{\text{int}} \qquad (9)$$

This linear approximation dramatically simplifies the fit.

Considering the duplex in solution, the dimer presence is likely to induce more subtle changes, such as increasing the rate of base pair opening, and thus imino proton exchange. We hypothesize that the hydrogen bond disruption from the formation of the lesion results in an increased rate of imino proton exchange from the involved thymine bases. In our experiments, a 10-mer oligonucleotide duplex is examined via NMR methods to examine rate of imino exchange by an ammonia exchange catalyst.

3. MATERIALS AND METHODS.

3.1. Buffer Preparation

Experiments were carried out in an NMR buffer of 100 mM sodium phosphate and 50 mM NaCl at pH 7.5. The buffer was prepared using dH_2O purified by a MilliQ Millipore filtration system. All chemicals used to prepare the buffers were purchased from Fischer or Sigma Aldrich.

For the HPLC purification, 100% acetonitrile is used with filtered 25 mM ammonium acetate buffer at pH 7.5.

For ammonia, the constant k_D is about 1.0 $x10^9$ $M^{-1}s^{-1}$, the pK_a of guanine is 9.5, and the pK_a of thymine is 9.9, while the pK_a of the first dissociable proton on the dimer is 10.65. For thymine k_B is 1.8×10^8 $M^{-1}s^{-1}$, for guanine k_B is $3.6\times10^8 M^{-1}s^{-1}$, and for the thymine dimer, k_B is 0.38×10^8 $M^{-1}s^{-1}$.

3.2. Sample Preparation

Unmodified DNA oligonucleotides were commercially synthesized by phosphoramidite synthesis by Integrated DNA Technologies. The oligonucleotides were obtained lyophilized in single-stranded form and purified using reverse phase HPLC on an Agilent Technologies 1100 HPLC, with a reversed phase 189.4 mm x 25 cm Zorbax Eclipse XDB-C18 column. A 25 mM ammonium acetate aqueous buffer at pH 7.4 is used as an eluent with acetonitrile to buffer against rapid pH changes. The flow was set to 3.7 mL/min and the maximum pressure is 350 bar. The oligonucleotides elute at roughly 12 minutes at a 89.28% aqueous phase (ammonium acetate buffer)

and 10.7% acetonitrile, indicated by a tall, thick peak appearing at an absorbance of 260-280 nm. For all the oligonucleotides used, the percent aqueous phase was varied in a linear gradient between 95%-80%, with a low percentage of acetonitrile. Single-stranded oligonucleotides containing a thymine dimer were commercially synthesized by solid-phase phosphoramidite synthesis by Midland Certified Reagent Company. The thymine-dimer containing oligomers were purified by HPLC by Midland and certified through ESI mass spectrometry. Following HPLC purification, samples were lyophilized with a Labconco Freeze Dry System/Freezone 4.5 instrument, and resuspended in NMR buffer (see above). NaCl content was originally reduced from 100 mM to 50 mM to enhance the NMR spectra. Increased salt content adversely affects the spectra by increasing line broadening. (*25*) The DNA samples were dialyzed overnight at 4°C in 1X NMR buffer to reduce the residual ammonium and acetate content from lyophilization. The DNA samples were divided into aliquots of 100 μL and then dialyzed with GE Healthcare Mini-dialysis tubes (250 μL) at a 1 KDa cutoff. Complementary strands were annealed by heating equimolar amounts to 90°C on a heat block and cooling slowly to room temperature for 3 hours.

The concentration of duplex DNA was measured using a Varian Cary50 Bio UV-Visible spectrophotometer at 260 nm using a 1 cm path length in a quartz cuvette. Concentrations were found using Beer's law using the extinction coefficients provided by IDT/Midland in Table 1.

Table 1. Extinction coefficients.

Oligonucleotide Strand	Extinction Coefficient (L/mol*cm)
KK3	95,200
KK4	104,000
KK3T<>T	77,000
KK5	106,300
KK6	121,700
KK5T<>T	88,700

Ammonia exchange catalyst solution was made up in a 4M stock. Aliquots of 100 μL DNA samples in phosphorus buffer were dialyzed overnight against 1L of 40 mM ammonia buffer at 4°C. To achieve higher catalyst concentrations of 80 mM, 100 mM, 120 mM and 200 mM, small volumes of 4 M ammonia stock were titrated directly into the NMR tube and mixed by pipetting. We titrated directly into the NMR tube to preserve the concentration of DNA. Excessively pipetting the DNA sample would leave residual sample on pipette tips, eventually decreasing the concentration of DNA. Peak height in the NMR spectra is a function of proton concentration, and we would observe shortening of the peaks with sample loss, interfering with our analysis of catalyst effect.

3.3 NMR Sample Parameters

NMR studies were performed on a Bruker AVANCE Ultrashield 400 MHz spectrometer, using a 5 mm broad-band inverse (BBI) probe with Z gradient. Samples were not spun. We completed one-dimensional and two-dimensional homonuclear ^{1}H-NOESY experiments in a 90% H_2O and 10%

D_2O 1X 100 mM sodium phosphate, 50 mM NaCl NMR buffer solution with a total volume of 450 µL and a DNA concentration of 700 µM. D_2O was purchased from Sigma Aldrich. A percentage of deuterium is required in the buffer even though it is not intended to label the DNA sample, because the NMR uses a deuterium frequency-field lock to prevent the drifting of the applied magnetic field B_0. The NMR constantly monitors the deuterium signal to maintain a constant frequency. Exchangeable and non-exchangeable protons were first determined by running 1D-^{1}H and 2D homonuclear ^{1}H NOESY experiments at 100% D_2O. 5 mm NMR tubes were used, by Shigemi Inc. All experiments were performed at 7°C. To ensure temperature control, the samples were stored in a modified Frigidaire wine refrigerator, which kept a constant 7°C. The DNA samples are sensitive to deviation from the desired 7°C; higher temperature would cause denaturation and the disappearance of imino signals in our NMR spectra. Dropping below 7°C causes cold denaturation, causing a similar distortion of the resultant NMR spectra. The melting temperature of the DNA samples is suppressed due to the shortness of the sequence and added presence of the dimer in KK3TT4. The pre-chilled samples were then placed into the pre-chilled NMR, which had been slowly cooled to 7°C.

All spectra were phased, cropped, Fourier-transformed and baselined in the NMR Pipe Suite of programs. Spectral processing was competed with MestReNova NMR software version 6.0.4-5850. The peaks were fit using a non-linear least squares fitting algorithm in Matlab (Mathworks, Natick MA).

3.4. NMR Instrument Parameters

We obtained one-dimensional spectra by a 1D pulse sequence provided by Bruker Avance version 02/05/31. The pulse program consisted of a single 90° pulse. Data acquisition of the free induction decay (FID) was obtained during the T2 relaxation. Water suppression was accomplished by a Watergate 3-9-19 pulse sequence with gradients. The number of scans was 512 and the time domain was 32768.

NOESY experiments were run with a pulse program provided by Bruker Avance version 00/02/07, 2D homonuclear correlation via dipolar coupling. The water suppression used a Watergate 3-9-19 pulse sequence with gradients. Mixing time was 0.15s, and the number of points was 2048, with 40 scans. The NOESY pulse sequence consists of three 90° pulses. The first pulse equalizes the energy level differences in the sample proton population through transverse magnetization. The pulse is followed by an evolution time (t_1) that allows the population nuclei to freely rotate, or precess, and the chemical shift of the nuclei is obtained. The second 90° pulse is in the Z direction. Mixing (τ_m), or longitudinal magnetization transfer between nuclei, follows. In NOESY, the magnetization transfer occurs through dipolar interactions, creating the nuclear Overhauser effect (NOE). The magnitude of the mixing time (τ_m) is chosen specifically to be close to the magnitude of the spin-lattice relaxation time (T_1). Mixing time is also kept constant throughout the NOESY. The third 90° pulse is in the XY plane, and data acquisition follows (t_2). During the data acquisition of the transverse magnetization, the

chemical shift of the nuclei is determined for the second time. The signals of the protons were recorded as a function of two transverse magnetization times t_1 and t_2. The two-dimensional Fourier transform gives a spectrum with two frequency axes, as opposed to the one-dimensional spectrum with intensity versus frequency (represented by chemical shift in parts per million).

Exchange rates were determined using magnetization transfer methods. Water protons were magnetically labeled by selective 180º inversion by a DANTE pulse sequence. The DANTE sequence contains a series of hard and soft pulses completed by a hard Z-gradient to eliminate transverse relaxation. Water suppression was accomplished with a jump-and-return sequence, based off of the experiments of Plateau and Guéron in 1982 (*24*). Time domain was optimized to 32000. With each exchange experiment, 40 separate NMR experiments were completed at a range of mixing times shown in Table 5. In experiment 1, water was referenced, and in experiment 2, water was inverted. Experiments 1 and 2 provide the data to calculate the efficiency of water inversion (E). Experiments 3-16 probed the inversion and recovery of water at a variety of mixing times to calculate water relaxation (Rl_w) as described in equation 5. The inversion-recovery experiment was first performed to account for the water's own relaxation to the Z-axis magnetic field created by the NMR, B_0. Experiments 17-40 applied a range of mixing times to elucidate the exchange rate for the imino protons. The exchange rate of the labeled water and the imino protons was obtained by measuring the intensity of the imino peaks as a function of mixing time. The imino peaks

were fit to an exponential function to determine the exchange rate, as described in equation 6. Experiments 1-40 were repeated for each catalyst concentration.

Table 2. Experimental process and mixing time.

Experiment Number Efficiency of Water Inversion (E)	Mixing Time (delay8)	Experiment Number Imino Exchange (k_{ex})	Mixing Time (delay8)
1	3s (Water Reference)	17	520 us
2	3s (Water Inversion)	18	600 ms
Water Relaxation (Rl_w)		19	10 ms
3	1.2 ms	20	150 ms
4	0.4 ms	21	1.5 ms
5	10 s	22	350 ms
6	1.6 s	23	500 ms
7	2.8 s	24	1 ms
8	3.6 s	25	250 ms
9	15 s	26	1.5 s
10	0.8 s	27	3 ms
11	3.2 s	28	75 ms
12	2 s	29	300 ms
13	4 s	30	20 ms
14	1.2 s	31	1 s
15	2.4 s	32	400 ms
16	6 s	33	100 ms
		34	750 ms
		35	200 ms
		36	450 ms
		37	50 ms
		38	2 s
		39	2.5 s
		40	1.75 s

4. RESULTS

4.1 Experimental Sequences

First we characterized a double stranded 12-base pair oligo-deoxynucleotide sequence KK56. The duplex sequence is shown in Table 3. The parent and dimer duplex structures are identical except for the addition of the *cis-syn* thymine dimer fusing T6 and T7.

Table 3. Sequence of 12-mer DNA Oligonucleotide Duplexes

Parent Duplex 5 and 6	
Strand 5	5'– C_1 C_2 G_3 T_4 G_5 T_6 T_7 A_8 T_9 G_{10} C_{11} C_{12}–3'
Strand 6	3'– G_{24} G_{23} C_{22} A_{21} C_{20} A_{19} A_{18} T_{17} A_{16} C_{15} G_{14} G_{13}–5'
Dimer Duplex 5TT and 6	
Strand 5TT	5'– C_1 C_2 G_3 T_4 G_5 $T_6 \bullet T_7$ A_8 T_9 G_{10} C_{11} C_{12}–3'[‡]
Strand 6	3'– G_{24} G_{23} C_{22} A_{21} C_{20} A_{19} A_{18} T_{17} A_{16} C_{15} G_{14} G_{13}–5'

[‡] The center dot represents the location of the *cis-syn* thymine dimer lesion site, such that T6 and T7 are fused by the cyclobutane ring.

We also characterized a second sequence, a double-stranded 10 base pair oligodeoxynucleotide with the sequence shown in Table 4, originally designed by John Stephen Taylor (*12*). Both duplex structures are identical except for the addition of the *cis-syn* thymine dimer. In the thymine-dimer containing 10-mer duplex, the lesion site occupies thymine 5 (T5) and thymine 6 (T6).

Table 4. Sequence of 10-mer DNA Oligonucleotide Duplexes, Taylor *et al.*

Parent Duplex 3 and 4	
Strand 3	5'– C_1 G_2 T_3 A_4 T_5 T_6 A_7 T_8 G_9 C_{10} –3'
Strand 4	3'– G_{20} C_{19} A_{18} T_{17} A_{16} A_{15} T_{14} A_{13} C_{12} G_{11} –5'
Dimer Duplex 3TT and 4	
Strand 3TT	5'– C_1 G_2 T_3 A_4 T_5 • T_6 A_7 T_8 G_9 C_{10} –3'‡
Strand 4	3'– G_{20} C_{19} A_{18} T_{17} A_{16} A_{15} T_{14} A_{13} C_{12} G_{11} –5'

‡ The center dot represents the location of the *cis-syn* thymine dimer lesion site, such that T5 and T6 are fused by a cyclobutane ring.

The parent complex (KK34) and dimer complex (KK3TT4) are non-palindromic and were selected based on well-resolved one-dimensional NMR spectra (Figure 10). A palindromic sequence was eliminated due to the possible formation of hairpin structures during annealing. The sequence was designed to be short in length, as a longer sequence would increase the number of imino proton signals and result in increased probability of peak overlap in the NMR spectra.

4.2 NMR Resonance Assignment

We used NMR spectroscopy during multiple stages of the experiment. We obtained one-dimensional spectra of the sequences to acquire a snapshot of the peak dispersion and resolution in the imino region, where "dispersion" refers to how much the peaks are spread out, and "resolution" to whether two neighboring peaks can be discerned as two separate signals. We used exchange experiments to determine the rate of exchange (k_{ex}) by fitting the one-dimensional spectra to Equation 6. We assigned the peaks of the 1D to

specific residues in the sequence from the two-dimensional homonuclear NOESY experiment. The two-dimensional NMR experiment shows through-space couplings that can reveal the DNA sequence. COSY (correlation spectroscopy) experiments reveal the through-bond, scalar couplings between neighbors. In contrast, NOESY (Nuclear Overhauser Effect Spectroscopy) experiments reveal the through-space, non-scalar interactions between protons that are less than ~ 6Å apart.

We identified exchangeable and non-exchangeable imino protons through spectra collection in deuterium oxide (100% D_2O) in 100 mM phosphate buffer. In pure deuterated solvent, amino and imino hydrogens on the duplex exchange with solvent deuterons, and the NMR signals associated with these hydrogens disappear on the resultant spectra. Deuterium has a unique magnetic moment compared to hydrogen, and since the instrument is tuned to pick up the resonance frequency of hydrogen, deuterium-labeled sites produce no detectable signal. The purely deuterated solvent samples served as a reference to the water samples. The focus of our study is the imino protons in the center of the DNA duplex, which are only available to the solvent during base pair opening. The 100% D_2O spectra show only the sugar and aromatic base protons. In 95% water, the exchangeable imino base protons were sequentially assigned through Nuclear Overhauser Effect (NOE) cross-peaks in the 11-13 ppm region of the spectrum between neighboring imino protons on adjacent bases. These assignments were confirmed by connectivities to aromatic and sugar proton regions. The two-dimensional

homonuclear ^{1}H-NOESY spectrum imino region was assigned for both parent (non-dimer-containing) and dimer-containing complexes. The connection of the sequential NOE connectivities, the "NOE walk", was completed following the H1 imino protons of guanine and the H3 iminos of thymine along the sequence. Numbering conventions follow standard guidelines.

We completed the NOE walk for the imino region of the 2D homonuclear ^{1}H-NOESY spectrum. Only thymines and guanines contain an imino proton, so only these residues appear in the 11-13 ppm region of the full spectrum. From this region, we completed an NOE walk following the neighboring thymine and guanines, in accordance with our sequence, along the stacked base at the core of the DNA duplex, shown in Figure 8.

A conventional NOESY spectrum features a diagonal series of peaks, representing the NOE internal NOE signals from a single base with itself. The diagonal is a topographical view of the one-dimensional spectrum, represented commonly as a contour plot. Regions of closely spaced lines indicate a sharp rise in topography, and widely spaced lines show flatter regions. On both sides of the diagonal, cross-peaks representing signals to neighboring bases are noticeable, with the pattern of cross-peaks symmetrical about the diagonal. From our sequence, we expect a diagonal consisting of ten residues for the KK34 duplex, corresponding to ten guanines and thymines, and a diagonal of twelve residues for the KK56 duplex.

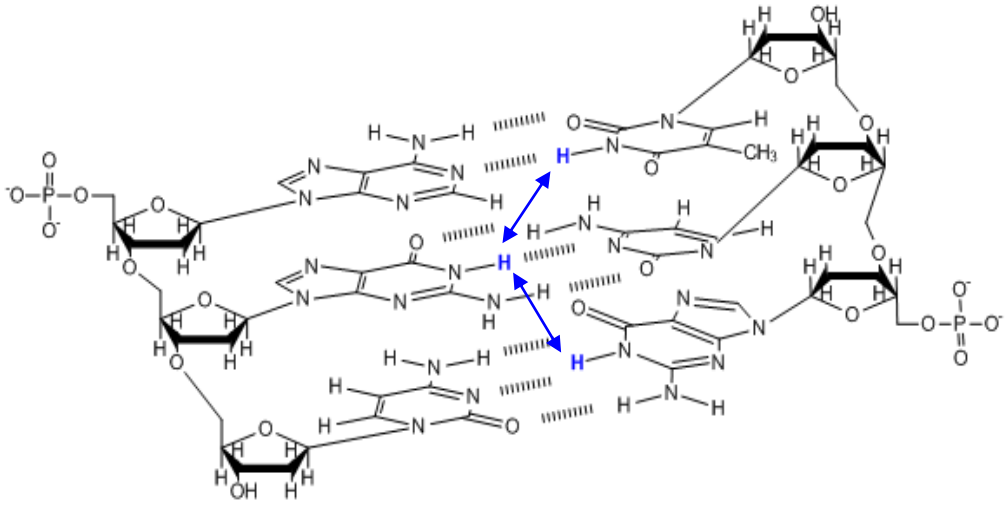

Figure 8. Sample diagram of a trimer 5'- A G C -3'. The imino proton for each complete base pair and the NOE interaction between them is highlighted in blue. A NOESY spectrum of the imino region would reflect the NOE interaction between each imino proton with the neighboring imino proton directly above or directly below.

4.3 One-Dimensional Spectra

To predict the peak dispersion in the two-dimensional experiment, we obtained one-dimensional ^{1}H-NMR spectra for the 12-mer and 10-mer parent and dimer complex. The full one-dimensional spectrum for the parent KK34 is shown below (Figure 9). Several key features can be elucidated from the spectrum, indicating correct data acquisition by the NMR experiment. The most obvious feature of the spectrum is the solvent peak, which in our case is water, at about 4.6 ppm. The tall, jagged peaks between 4.5 and 4.6 ppm indicate that the water suppression pulse sequence is working, and the tallest, most intense region of the water peak has been largely cancelled out. The Watergate water suppression technique pulses the solvent 90° to the X-Y plane, followed by a delay time (τ), followed by a second 90° pulse returning the solvent signal to the Z-axis. The technique effectively cancels the water signal, so that the peak displayed during data acquisition is "squashed". Without the technique, the water signal, which is present in a 10^6 :1 ratio with the DNA solute, would be so enormous that it would distort the baseline, and the DNA peaks would be lost in the feet of the water signal. In the figure below, the water peak is suppressed and the baseline is horizontal, with very little noise compared to the DNA signals. For DNA, the spectrum is expected to include the presence of tall methyl peaks (~1-1.5 ppm), a range of sugar peaks (1.5-2.5 ppm), and nitrogenous base peaks. On the bases, the amino and aromatic ring protons should appear in the 6.5-8.5 ppm range, and the imino protons should be isolated in the 11-13 ppm range, much farther downfield than the majority of the signals.

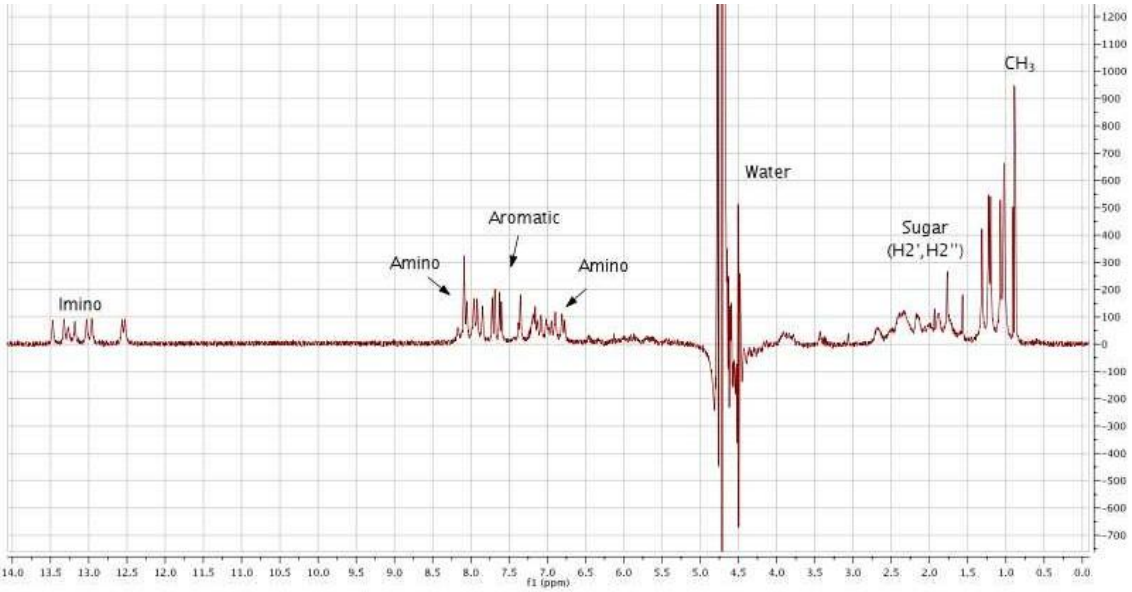

Figure 9.1D spectrum of KK34, the parent strand, (90% H_2O 10% D_2O 1X 100mM phosphate NMR buffer at 7°C) with typical regions of a DNA spectrum labeled.

From the full spectrum of KK34, regions typical of a DNA oligomer are indicated. The thymine methyl protons, identified by an upfield, characteristic triplet, are strongly observed at 0.8 ppm. We expect the sugar protons H2' and H3' in the region of 2-2.5 ppm, and although the peaks were not explicitly assigned, characteristic peaks can be identified in that region, with some overlap. H4', H5' and H5'' are expected at 4-4.5 ppm. H4', H5' and H5'' are often observed to have poor dispersion and further two-dimensional COSY or TOCSY experiments would be needed to clarify the signals. The water peak at 4.7 ppm is suppressed, but the signal is still large enough to interfere with the sugar protons H1' and H3', which would be expected downfield of water, at around 5.7 and 5 ppm respectively. Amino protons from cytosine, guanine and adenine are visible flanking the aromatic ring protons. The aromatic region, previously assigned by John Stephen Taylor for this sequence, was not assigned here. (*12*) As the furthest observable downfield cluster of signals, the resolution of the imino region is not impeded by any other interfering signals.

We collected one-dimensional spectra for each sequence. The imino region (11-13 ppm) was isolated using Bruker Topspin, and the peaks in the region were hand phased and evaluated for the characteristics of dispersion and resolution. The peaks could not yet be assigned to thymine and guanine residues; the assignment comes from the two-dimensional NOESY. A sample unassigned region of KK34 is shown below. (Figure 10)

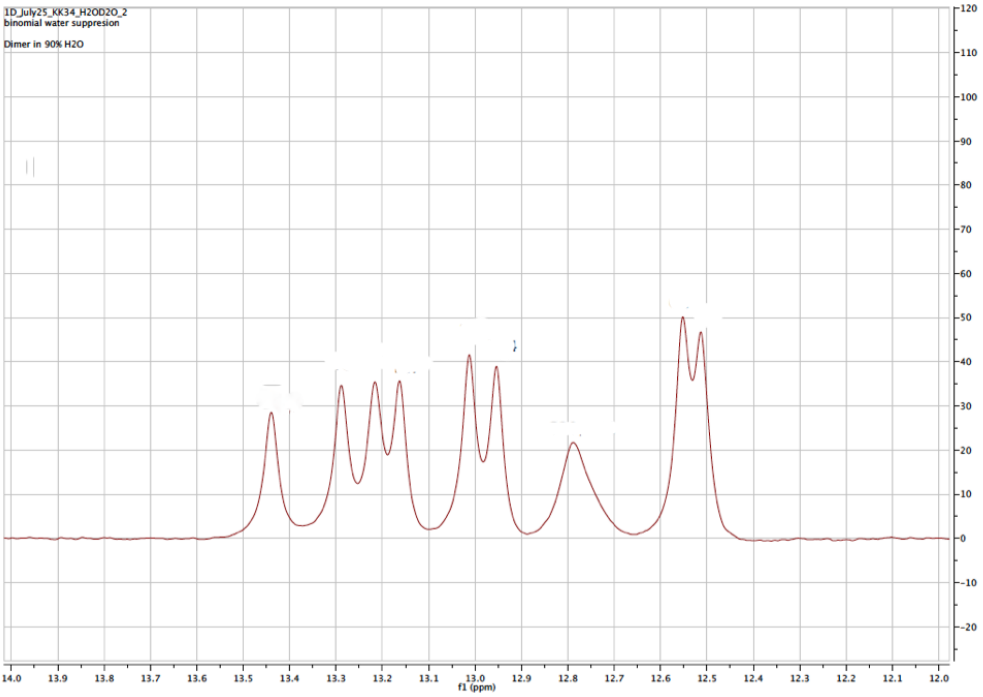

Figure 10. Imino region of KK34, with no assignment. Peaks are well resolved, with nine individual peaks, including one short, broad peak probably corresponding to the end residues.

4.4. Two-Dimensional NOESY Spectra

As previously discussed, NOESY is a 2D NMR technique that reveals Nuclear Overhauser Effect (NOE) interactions between nuclei, represented as a cross-peak on the spectrum. NOE's are observed between nuclei in a non-covalent, through-space interaction, as their resonances interact in the magnetic field. Following the cross-peak connectivities can indicate the spatial configuration of the atoms in the molecule.

The two-dimensional homonuclear ^{1}H- NOESY experiment of the KK56 parent reveals the cross-peaks between the residues (Figure 11). At first inspection, the imino peaks are very well resolved. The diagonal, which represents the NOE interactions of the residues with themselves, has sharp points, and the center of each peak is easily identified. The two-dimensional NOESY spectrum can be viewed as a topographical contour plot of the one-dimensional spectrum, with the addition of symmetrical cross-peaks indicating NOE interactions about the diagonal. The symmetry indicates good phasing. The noise of the spectrum is very low, as evidenced by the complete assignment of all cross-peaks off the diagonal. The ability to follow the NOE interactions from G23, to G3, to T4, etc, to the last residue G14, indicates that the DNA sample is annealed. The ends are not observed, but they can fray in solution and lose their neighboring protons to the solvent on the timescale of the NOESY experiment.

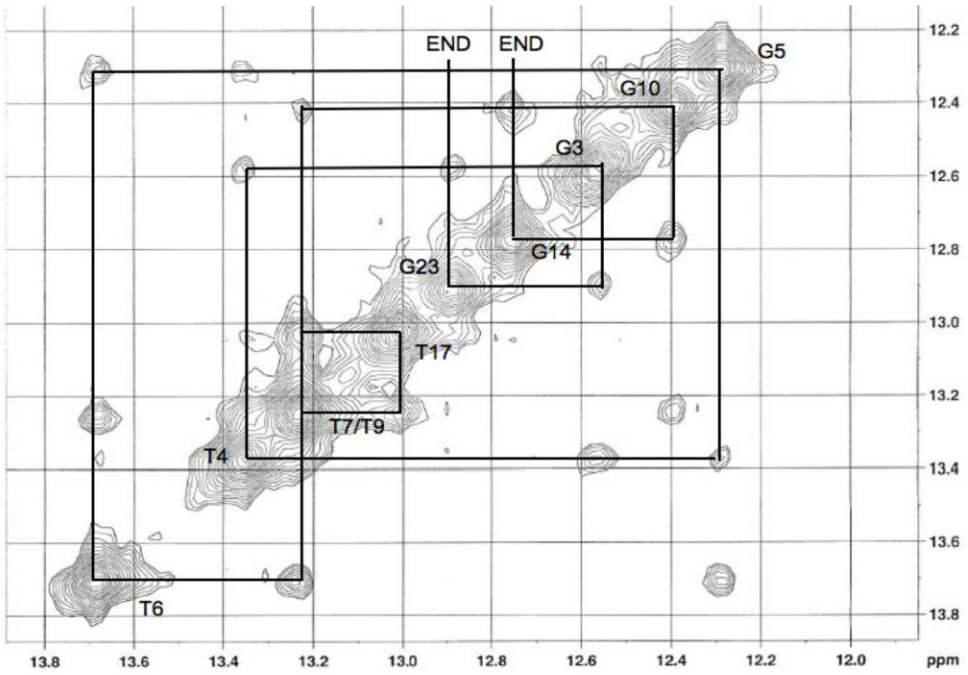

Figure 11. Expanded imino proton region (12-14 ppm) of 2D NOESY spectrum of KK56 d(CCGTGTTATGCC)•d(GGCACAATACGG), in 90% H_2O 10% D_2O 1x NMR buffer at 7°C. The path indicates the NOE walk, or the successive imino protons. For example, T6 has cross-peaks to T7 and G5, as we would predict from the sequence (Table 3).

The two-dimensional homonuclear NOESY of KK5TT6 (Figure 12) is less sharp compared to the parent NOESY. The signals of the cross-peaks are much shorter than the signals in the diagonal. In order to see the cross-peaks at all, we lowered the threshold significantly, allowing bands of noise to appear on the spectrum as smears at 12.8, 12.55 and 12.1 ppm. Toggling the threshold could eliminate the noise to produce a clean spectrum, but some of the cross-peaks would have been lost. Since the noise floor was lowered, the peak tips of the diagonal are truncated. To perform the NOE walk, two separate spectra were used; one spectrum containing the peak tips and one spectrum containing the complete set of cross-peaks. Due to the limitations of Bruker Topspin, the two spectra could not be overlaid, and instead had to be manually compared. Only the spectrum containing the complete set of cross-peaks is shown below.

In comparing the parent to the dimer, the thymine dimer 5' T6 residue is a strong, clear signal farther upfield than all of the guanines in the sequence, and has shifted significantly from its position in the parent. The NOESY also highlights the clustered overlap of G23, T17, G14 and T7. T4 and T9 are overlaid, and in the case of G14 and T7, the cross-peaks indicate very slightly different positions to the peak, but the resolution of the spectrum was too poor to adequately distinguish the two. There is some overlap at the base of G10 and G5, but the peaks appear to be sufficiently resolved.

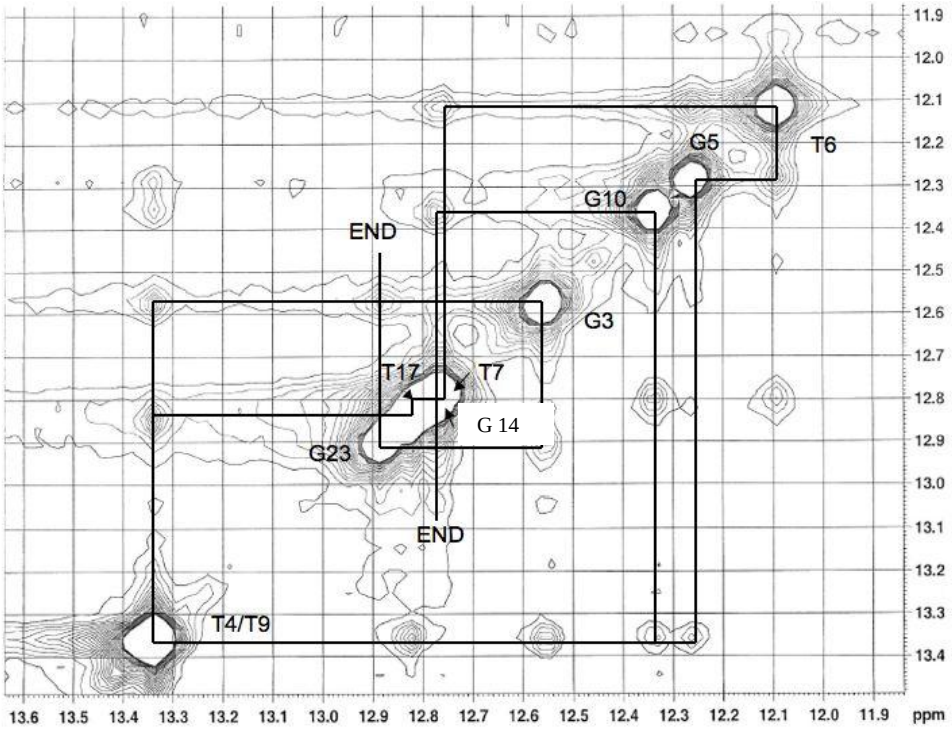

Figure 12. Expanded imino proton region (12-14 ppm) of 2D NOESY spectrum of KK5TT6 d(CCGTGT<>TATGCC)•d(GGCACAATACGG), in 90% H_2O 10% D_2O 1x NMR buffer at 7°C. The path indicates the NOE walk, among the imino protons. For example, T6 has cross-peaks to G5 and T7. Smears of noise are noted at 12.8, 12.55 and 12.1 ppm.

In two-dimensional homonuclear NOESY of KK34 (Figure 13), similarly to the KK56 sequence, we attributed peaks to each of the non-end thymine or guanine residues. We did not observe diagonal peaks for the end guanines involved in the termini base pairs C1•G20 and C10•G11, due to fraying in solution and rapid exchange with water. It is possible the gap in between T14 and G2 contains the end peaks, but they might be too short and broad to appear on the spectrum with a minimum intensity threshold set to eliminate background noise. They could also be under other peaks, but it is hard to tell from the two-dimensional spectrum alone; the intensity is difficult to evaluate by the contour lines, and presently all the peaks on the diagonal are intense. The one-dimensional spectrum we acquire later will aid in solving the dispersion issue. The residues G2 and G9, and T3 and T17 are closely clustered, but we can still resolve the peak apexes from the contour plot, and these appear to be sharp. The cross-peaks in the KK34 spectrum are also much shorter than the diagonal peaks, and we lowered the noise threshold to resolve them. As a result, bands of noise are vaguely present at 13.0 and 13.35 ppm. However, the resolution of the cross-peaks is sufficient to differentiate them from noise peaks.

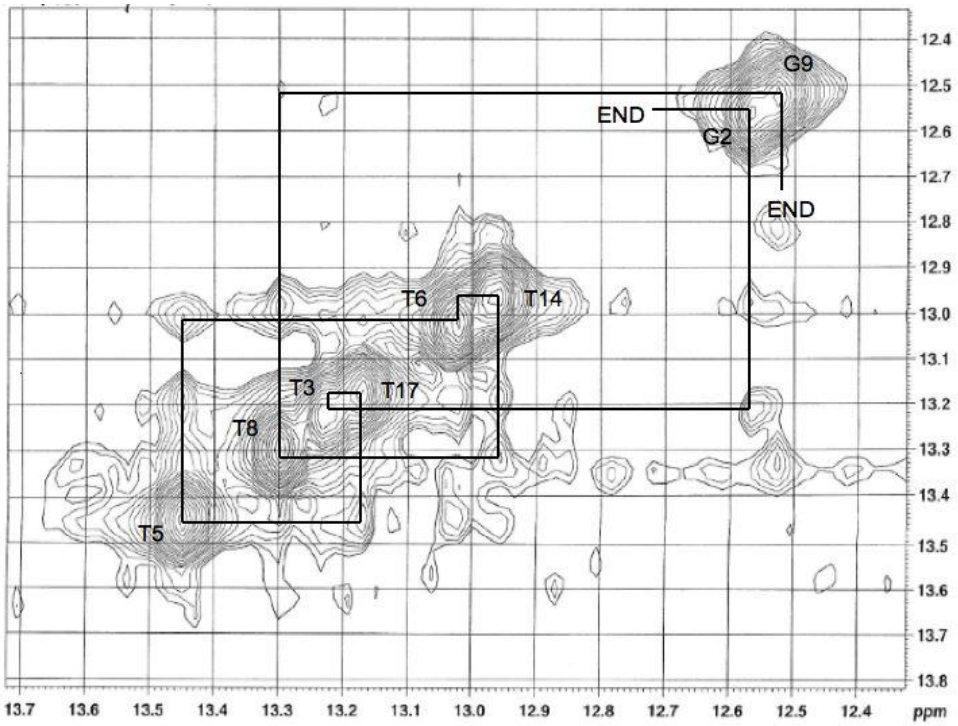

Figure 13. Expanded imino proton region (12-14 ppm) of 2D NOESY spectrum of KK34 d(CGTATTATGC)· d(GCATAATACG) in 90% H_2O 10% D_2O 1x NMR buffer at 7°C. The path indicates the NOE walk, or the successive imino protons. For example, T6 has cross-peaks to T5 and T14. Noise appears at 13.35 and 13.0 ppm.

The two-dimensional homonuclear NOESY of KK3TT4 (Figure 14) produced an observable change from the parent NOESY, confirming the presence of the dimer in KK3TT4. The loss of aromaticity to T5 and T6 caused upfield shifts of both resonances, but with a larger difference observed in T5. T5 is shifted much farther upfield (11.78 ppm) from the normal chemical shift range of a canonical Watson Crick A•T basepair (*26*). T6 has a smaller chemical shift change compared to T5, but its position is again closer to the guanine residues than would be expected for a canonical A•T basepair. The ends are again unresolved but they may be between T14 and G2 at 12.75 ppm, as expected from the parent. The ends are likely to be buried under the much stronger T14 and T6 signals. T14 and T6 appear to be tightly clustered, but there is no significant interference. We observed that the T3 and T17 resonances shift from the parent complex. Both T3 and T17 residues are on the 5' side of the dimer, which suggests a greater perturbation upstream from the dimer than downstream. The effect is supported by the relative lack of movement of T8, the only thymine residue on the 3' side of the dimer.

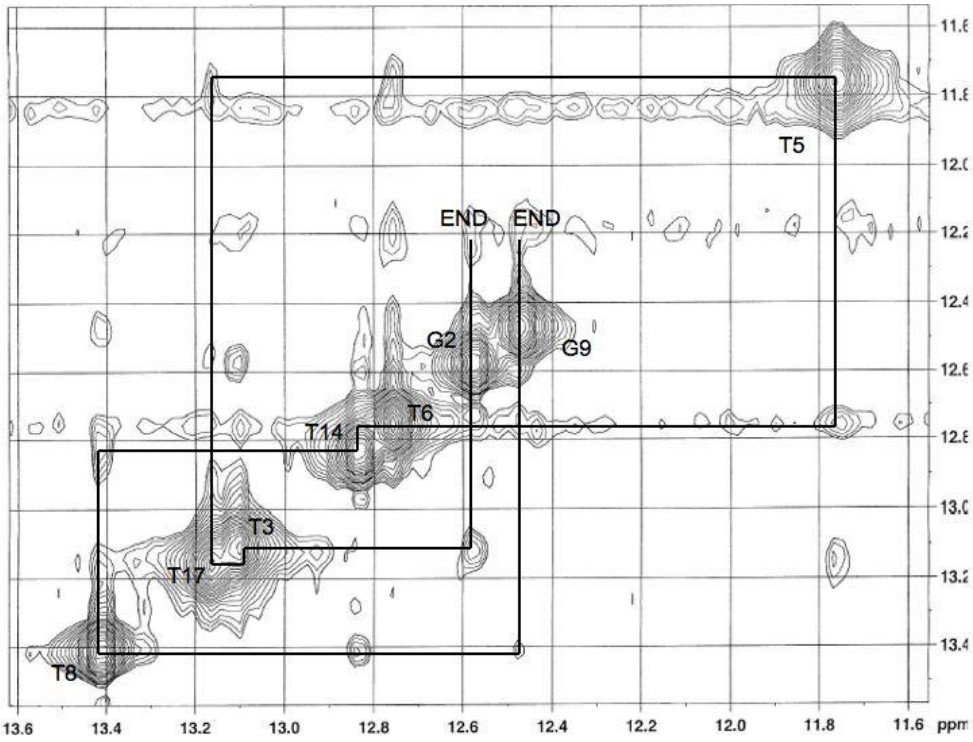

Figure 14. Expanded imino proton region (12-14 ppm) of 2D NOESY spectrum of KK3TT4, d(CGTAT<>TATGC)· d(GCATAATACG) in 90% H_2O 10% D_2O 1x NMR buffer at 7°C.

4.5. Assigned One-Dimensional Spectra

Using the data from the NOESY experiments, we assigned the sequential connectivities to cross-peaks and diagonal peaks to residues in the sequence.

We sequentially assigned the KK56 parent peaks from an expansion of the imino region (Figure 15). Superficially, nine distinct peaks are visible. For a 12-mer we expect 12 peaks, which suggests that one or more peaks represent more than one residue. The peak height is homogenous, consistent with the fact that the intensity of the signal is directly proportional to the number of protons. The peaks at 13.25 and 12.55 ppm are roughly double the height of the neighboring signals, which we interpret as the peaks that represent multiple residues. However, the peaks appear well dispersed on first impression, and we observe little overlap. The critical residue of T6, which will later be involved in the thymine dimer lesion, is neatly isolated at 13.7ppm. The signal to noise ratio is very good, and we observe that the baseline is completely horizontal with the DNA peaks rising up sharply.

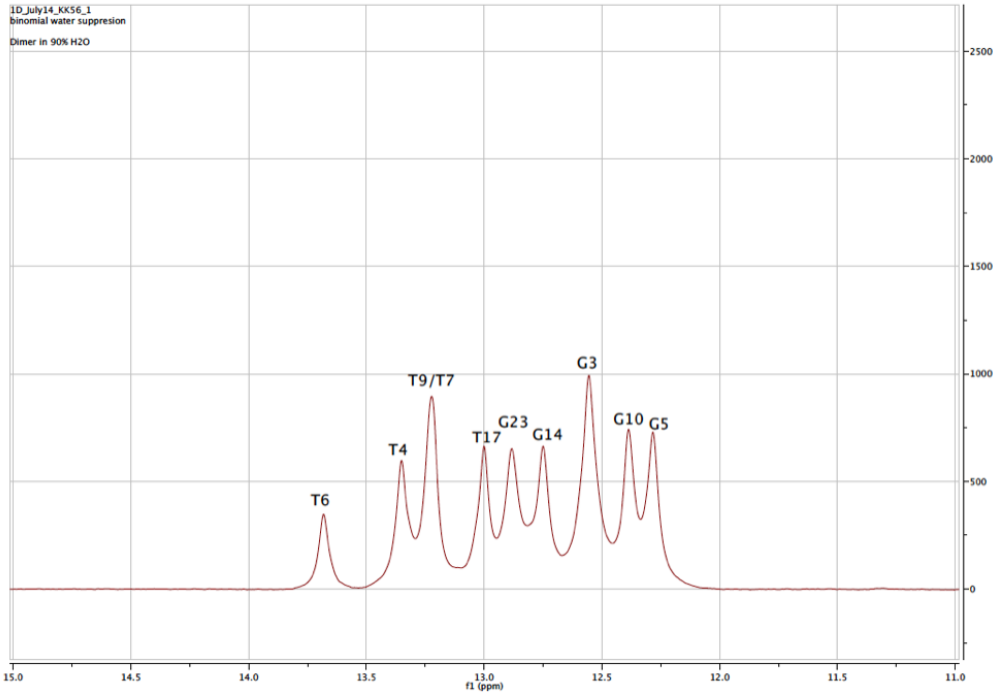

Figure 15. 1D spectrum of imino proton region (12-14 ppm) of the parent strand KK56, d(CCGTGTTATGCC)•d(GGCACAATACGG), in 90% H_2O 10% D_2O 1x NMR buffer at 7°C.

Even though the isolation of T6 is ideal, we observe T7 is overlapped with T9. The T7/T9 peak also partially overlaps with the T4 residue. T7, T9 and T4 are all towards the center of the sequence, and have very similar electronic environments. Towards the center of the imino region, T17, G23 and G14 are spaced very closely, and the three signals overlap significantly close to the baseline. Even though each signal is clearly resolved, the peaks themselves are grouped tightly. When exchange catalyst is added, we expect these peaks to broaden, and the tight cluster of signals could prove problematic once the secondary experiments are performed, since we want to obtain rate constants for every residue. T17 is buried in the center of the sequence, and has the furthest upfield shift, as expected. G23 and G14 are the penultimate bases in the sequence, and we expect them to have very similar chemical environments. G3 is uncharacteristically intense for a single residue signal, compared with a signal like T6. We interpreted the intensity of the signal to contain the unassigned end bases, G23 and G13. The residues are buried underneath, increasing the number of protons represented and significantly adding to the peak height. We expect the end residues to be missing or too broad to be defined based on the consistent lack of end residues in the parent/dimer sequences. G5 and G10 are the furthest upfield signals, corresponding to residues buried close to the middle of the sequence.

We acquired one-dimensional spectra for the dimer duplex KK5TT6 (Figure 16). In comparing the imino region of the parent and dimer 12-mer duplex spectra, we observed the thymines associated with the dimer (T6 and

T7) exhibit noticeable shifts in frequency. In the dimer complex, T6 migrates 1.58 ppm upfield, compared to its position in the parent. T7 migrates a shorter distance, but the residue does shift 0.46 ppm upfield. In the parent spectrum, T6 is the furthest downfield peak, and in the dimer strand, T6 is the furthest upfield, surpassing the normal range for thymine residues, and even guanine residues. Previous studies document a significant upfield shift of the dimer residues, so the T6/T7 shift confirms the presence of the dimer in our sequence. The isolation of T6 from the other peaks on the diagonal is ideal for subsequent peak fitting, especially paired with its isolation in the parent duplex. However in both the parent and dimer sequences, T7 is overlaid with a second peak. In the parent, T7 and T9 overlap, and in the dimer, T7 and G14 are overlaid. The position of T7 is not ideal, especially compared with the clarity of T6. Additionally, G23 and T17 are almost completely overlapping with the G14/T7 peak, and the broadness of these peaks close to the baseline suggest that the ends are buried underneath. Similarly G10 and G5 are partially overlapping and T4 and T9 are completely overlapping. The vast majority of the peaks in sequence KK56/KK5TT6 will be extremely difficult to resolve and fit once they broaden in the presence of exchange catalyst.

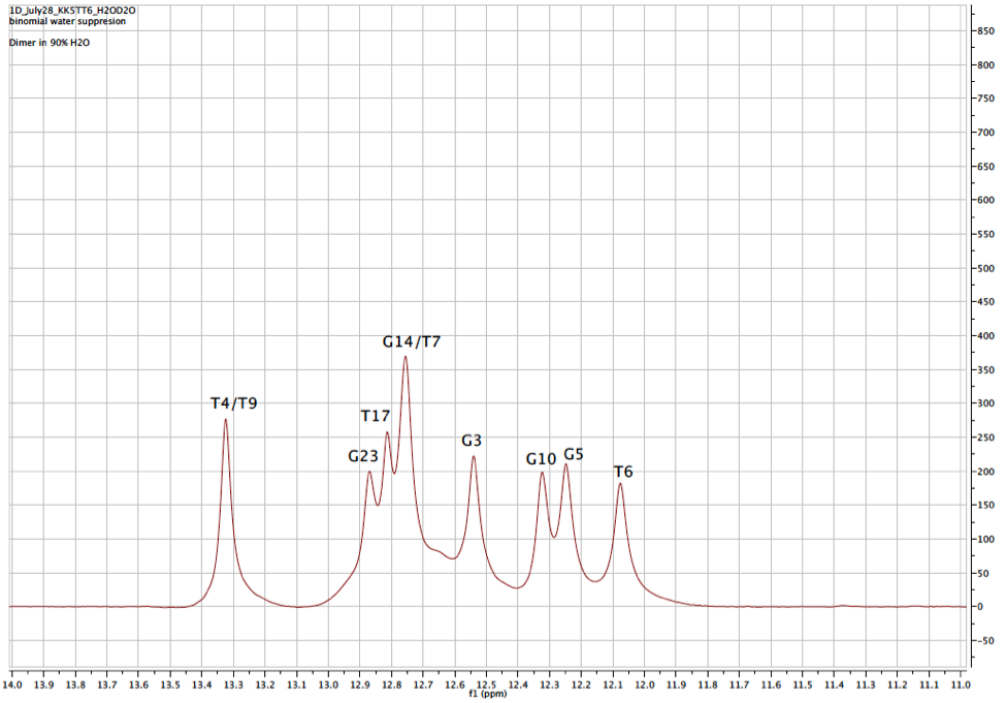

Figure 16. 1D spectrum of imino proton region (12-14 ppm) of the dimer strand KK5TT6, d(CCGTGT<>TATGCC)•d(GGCACAATACGG), in 90% H_2O 10% D_2O 1x NMR buffer at 7°C.

A summary of chemical shifts we observed is in Table 5 below.

Table 5. Chemical shifts (in ppm) of imino proton resonances in the parent (KK56) complex versus dimer complex (KK5TT6).

Base	Parent (KK56) -NH	Dimer (KK5TT6) -NH	Δppm
G24	12.57	12.58	0.01
G23	13.90	12.87	-1.03
G3	12.57	12.57	0.00
T4	13.35	13.37	0.02
G5	12.10	12.26	0.16
T6	**13.70**	**12.09**	**-1.61**
T7	13.23	12.74	-0.49
T17	13.01	12.83	-0.18
T9	13.23	13.37	0.14
G10	12.40	12.33	-0.07
G14	12.76	12.77	0.01
G13	~ 12.75	(un-resolved)	N/A

Due to the overlapping problems of the critical T7 residue in the KK56/ KK5TT6 sequence, we considered the sequence of KK34/KK3TT4. The sequence was shortened by two base pairs to decrease the overlap and remedy the crowding of the imino signals. The KK34 sequence was originally studied by John Stephen Taylor *et al.*, and the two-dimensional spectrum has been previously solved in the aromatic region, but notably not in the imino region.

The one-dimensional spectrum imino region of KK34 (Figure 17) coincides with our expectation of at least eight distinct peaks for the sequence.

We resolve nine peaks, but the ends are expected to have poorly resolved peaks, which is consistent with the 2D spectrum. We assigned peaks to each of the six thymine residues, and two of the four guanine imino peaks. The guanine peaks are tall, but not so tall as to expect the peaks to represent multiple residues. The 1D shows a broad, flat peak at 12.75 ppm, between T14 and G2, which can be attributed to the unaccounted guanines of the terminal pairs C1•G20 and C10•G11 pairs. In the case of KK34, the end peaks are distinct, and are not hidden under the peak of another residue.

Importantly, the spectra show that the thymines involved in the dimer, T5 and T6, are easily identified. We observe that T6 has some overlap with T14, but the peaks are sufficiently resolved. The thymine residues flanking T5/T6 have very similar chemical environments, indicated by the close proximity of their peaks (T8, T3, T17). G2 and G9 also contain a high degree of overlap, but the peaks are distinct and the behavior of the guanine residues is not critical to the experiment.

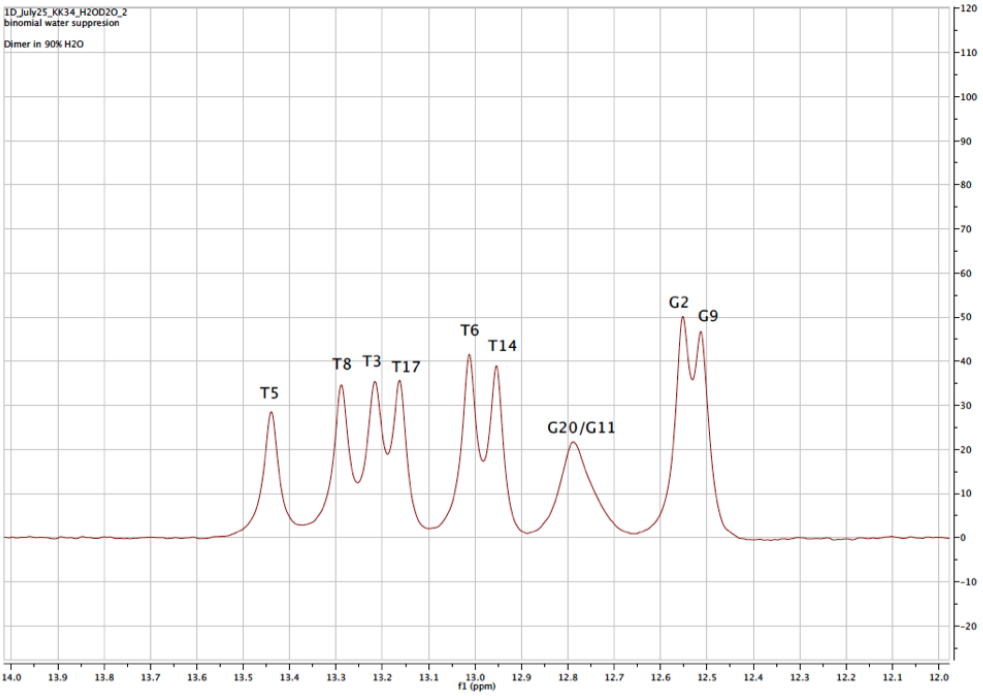

Figure 17. 1D spectrum of imino proton region (12-14 ppm) of the parent strand KK34, d(CGTATTATGC)• d(GCATAATACG), in 90% H_2O 10% D_2O 1x NMR buffer at 7°C.

We obtained one-dimensional spectra for the dimer duplex KK3TT4 (Figure 18). The imino region of the dimer duplex shares the same spectral resolution as the parent complex with little broadening of the signals. We attributed the minimum of eight peaks to each non-end residue. Importantly, we assigned the 5' end dimer-containing thymine, T5, to a peak abnormally upfield of the expected thymine and guanine region. Recall that in the KK5TT6 one-dimensional spectrum, the upfield-shifted T6 was at 12.1 ppm, close to the guanine residues. In KK3TT4, the upfield-shifted T5 is close to 11.8 ppm, and is within 0.6 ppm of the closest guanine residue, corresponding to a significant gap in the spectrum. The thymine fused to T5, T6, also has an observed upfield shift compared to the parent. T17 and T3 have very similar chemical environments as observed by a large amount of spectral overlap, but the peaks are just dispersed enough for sufficient resolution. T14 and T6 also share some overlap. T14 is almost double the heights of the neighboring peaks, so we can assume that the guanines in the end pairs of C1•G20 and C10•G11 are buried underneath.

A summary of the chemical shifts for the KK34/KK3TT4 exchangeable imino protons is listed below (Table 6). The T5 residue undergoes a 1.66 ppm shift upfield from parent to dimer, and T6 undergoes a 0.25 ppm upfield shift. The changes in chemical shift per guanine or thymine residue can be mapped onto a model of our sequence.

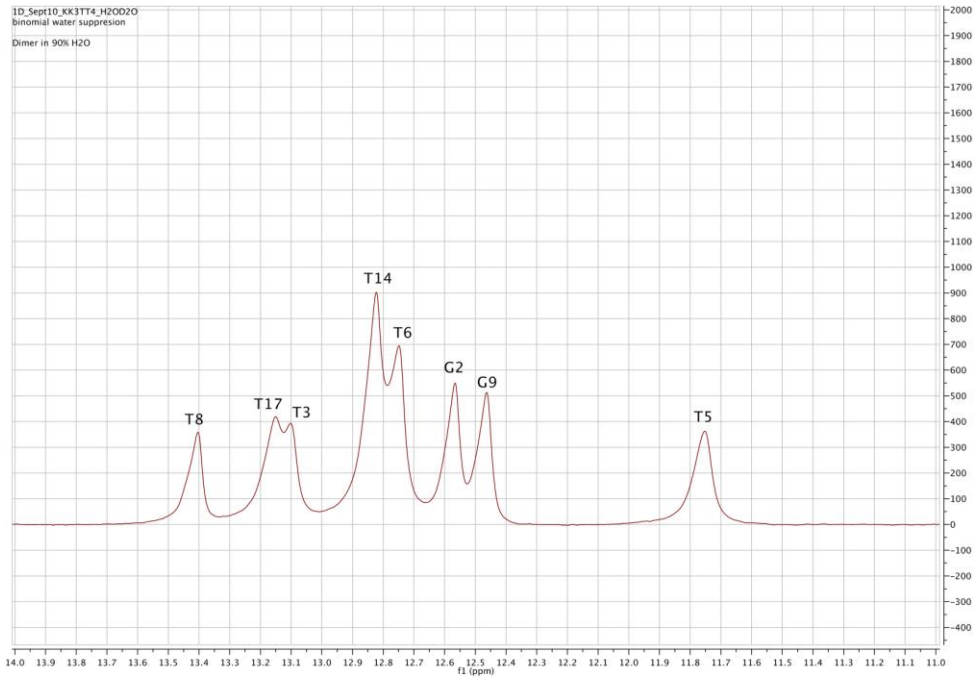

Figure 18. 1D spectrum of the expanded imino proton region (12-14 ppm) of KK3TT4, d(CGTAT<>TATGC)• d(GCATAATACG) in 90% H_2O 10% D_2O 1x NMR buffer at 7°C.

Table 6. Chemical shifts (in ppm) of imino proton resonances in the parent (KK34) complex versus dimer complex (KK3TT4).

Base, 5' → 3'	Parent (KK34) -NH	Dimer (KK3TT4) -NH	Δppm
G2	12.57	12.58	0.01
T3	13.23	13.1	-0.13
T5	**13.44**	**11.78**	**-1.66**
T6	13.02	12.77	-0.25
T8	13.3	13.4	0.10
G9	12.52	12.48	-0.04
G11	~ 12.75	(un-resolved)	N/A
T14	12.96	12.92	-0.04
T17	13.17	13.18	0.01
G20	~ 12.75	(un-resolved)	N/A

4.6. Exchange Experiments

To determine the rate of base pair opening, we used one-dimensional ^{1}H NMR to monitor changes in the imino region of the parent and dimer duplex in ammonia catalyst. We titrated ammonia directly into the NMR tube, and at each concentration, we obtained1D spectra at a range of mixing times. Initially, we referenced and inverted the water peak. From the inversion experiment, we obtained the efficiency of inversion, E. In the ideal case, the value of E is -2. We relaxed the water peak at a range of mixing times from 1.2 ms to 15 s. The intensity of the water peak (W) is plotted versus mixing time (Figure 19).

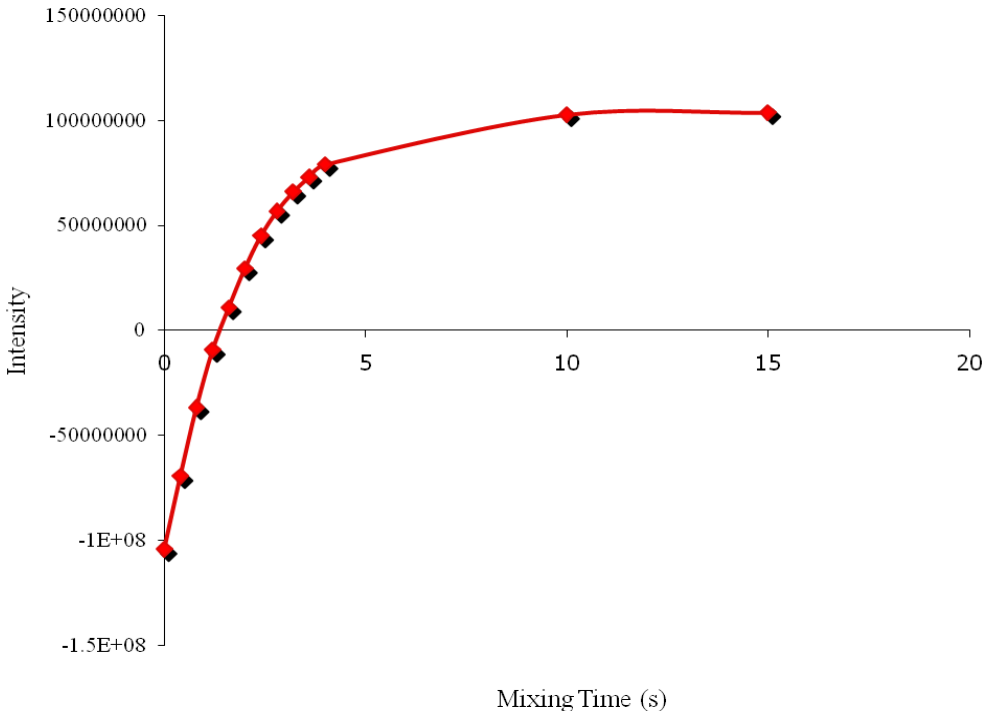

Figure 19. Water inversion. The trend indicates that the water peak is successfully inverted, and then relaxes back to the applied magnetic field B_0 (equilibrium) at full intensity, reaching a plateau with increased mixing time.

The water relaxation, Rl_w can be found using Equation 5.

$$W(x) = W_{eq} * (1.0 - E * e^{-xRl_w}) \qquad (5)$$

Where x represents mixing time, E is the efficiency of water inversion and Rl_w is the relaxation of water. The process is described by Equation 1, from which the efficiency of inversion, E, and the relaxation rate of the water protons, Rl_w, can be obtained. On our instrument, E ranges from -1.7 to -1.97, and Rl_w ranges from 0.46-0.55.

In solution, base pairs in the DNA duplex "breathe" and bases open periodically to the solvent. The previously bonded imino protons are exposed to the solvent, and the imino protons exchange with the inverted water protons with a rate k_{ex}, causing the peaks to decrease in height for about 0.5 s. Simultaneously, the water and imino protons relax with rates of Rl_w and Rl_i respectively (Eq. 6), and the imino peaks return to their original heights. The change in imino proton height as a function of mixing time is graphically represented in Figure 20. The amplitudes of the imino peaks change as a function of mixing time as base protons exchange with solvent protons.

At 40mM ammonia catalyst, the parent KK34 maintained excellent peak dispersion at a range of mixing times from 520 μs to 2 s. Line broadening did not interfere significantly with the peak resolution.

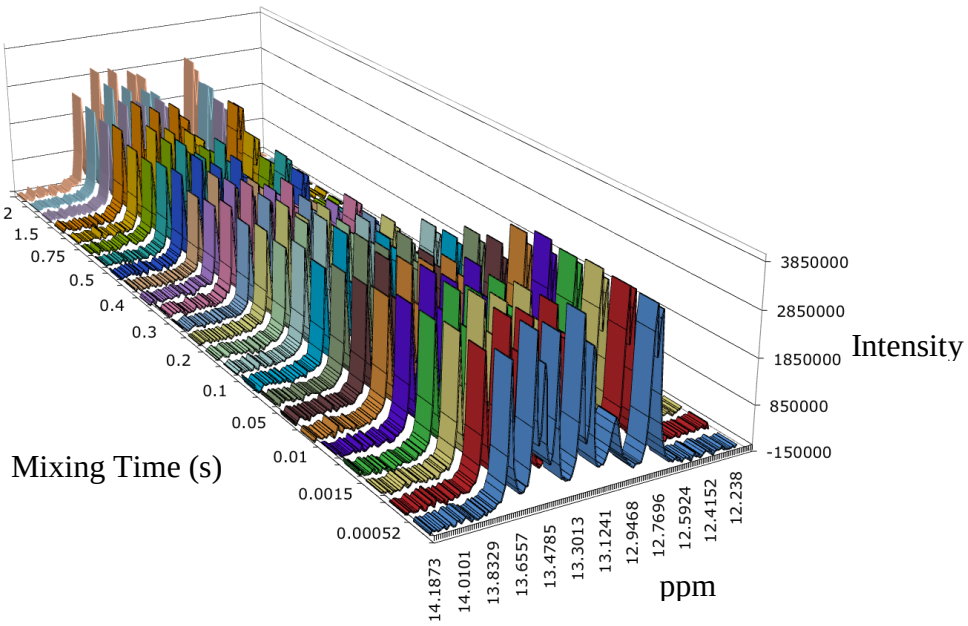

Figure 20. KK34 parent imino proton spectra as a function of mixing time, in 40 mM ammonia catalyst. The peaks change in intensity as a function of mixing time, reaching a minimum around 0.5 s. Note that spacing on the mixing time axis is not proportional to time.

A similar plot can be made for the dimer sample (Figure 21). In comparison to the parent KK34 imino proton spectra, the KK3TT4 dimer imino proton spectra rapidly decay in peak height with mixing time. The drop in peak amplitude is significant in the longer mixing times, around 0.5 s. At short mixing times (0.01 s), the peaks are at their greatest amplitude indicating that few protons have exchanged with the labeled water. The imino protons then recover in height at long mixing times (2 s). In the dimer sample at 40 mM ammonia catalyst, peak resolution became poor around 0.5 s, when line broadening distorted the peak resolution of the residues G2 and G9, at the center of the sequence. At 40 mM some peaks at the center of the sequence were slightly negative, these peaks likely correspond to the ends, which are already frayed and exchanging quickly with the solvent, as predicted by the two-dimensional and one-dimensional experiments.

At each increase in the catalyst concentration, we measured a series of one-dimensional spectra in the imino region over a range of mixing times. As the catalyst concentration increases, we expect existing imino peaks to decrease in height or disappear altogether in a quick relaxation to equilibrium.

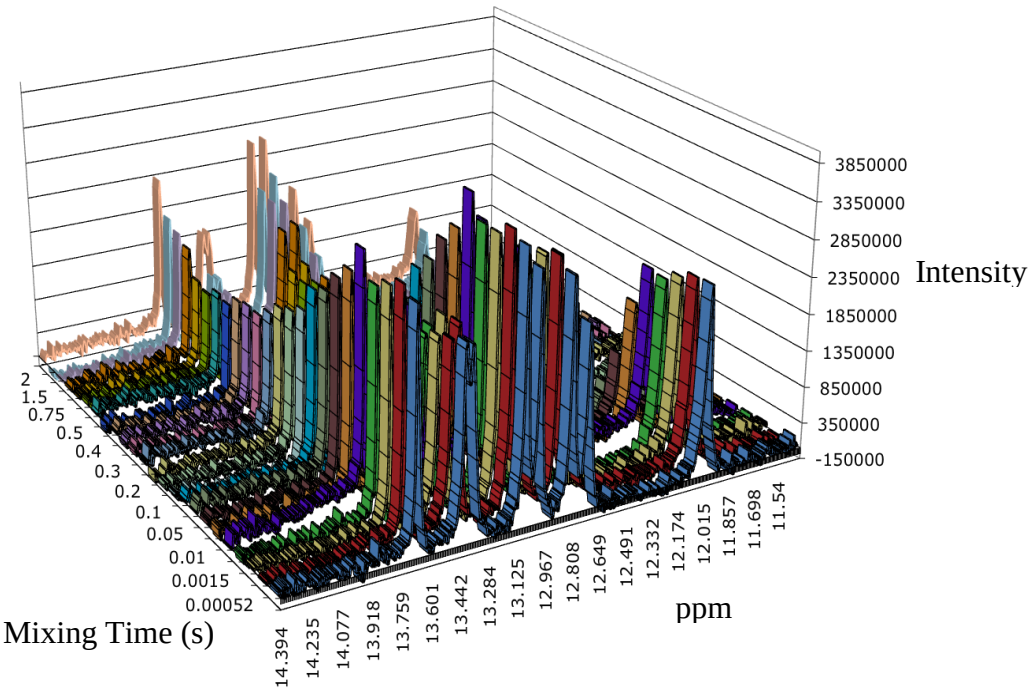

Figure 21. KK3TT4 dimer imino proton spectra as a function of mixing time, in 40 mM ammonia catalyst. The change in peak heights is observed at a range of mixing times, with some peaks at a negative intensity at 0.5 s.

Individual imino proton peaks can be more meaningfully represented in an exchange graph, with peak intensity as a function of mixing time. The curves generated for each imino peak can be fit to Equation 5, since we know the efficiency of water inversion (E). The equation fits the variables of the exchange rate (k_{ex}) and the imino proton relaxation rate (Rl_i).

We converted the stacked plot of one-dimensional imino region spectra to an exchange curve for KK34 (Figure 22) by integrating the area under each curve. The peaks are arranged in order of most downfield to most upfield. The broad, flat end peak observed in 100 mM phosphate buffer at 12.75 ppm, between T14 and G2, was not observed at 40 mM ammonia, due to rapid exchange. At a catalyst concentration of 40 mM ammonia, none of the parent imino protons were negative in intensity at any mixing time. All of the imino peaks follow the same trend in intensity with mixing time. The imino protons were observed to have a peak minimum at 0.5 s. At the short exchange times between 0 and 0.5 s, peak height rapidly decreased, and slowly recovered from 0.5 to 2.5 s.

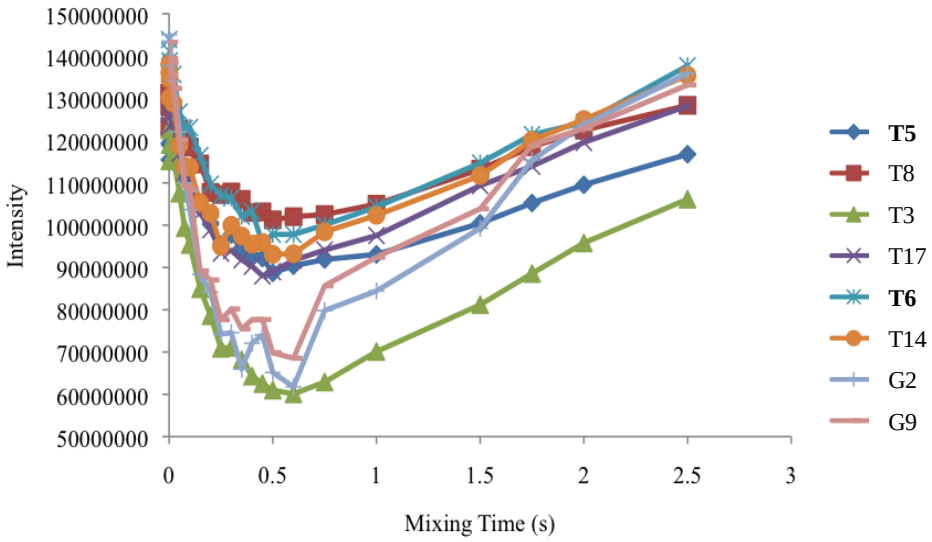

Figure 22. Individual imino protons of KK34 in 40mM ammonia catalyst. Peaks are labeled according to chemical shift. All of the imino residues remained positive throughout the range of mixing times. T3, G2 and G9 dropped to the lowest observable intensities.

We converted the stacked plot of the dimer KK3TT4 one-dimensional imino region spectra to an exchange curve (Figure 23). The peaks are numbered sequentially in order of most downfield to most upfield, reflecting the changes in chemical shifts of the residues from the parent sequence to the dimer. As in the parent, no end residues were distinguishable due to rapid exchange and overlap with the guanine resides G2 and G9. At a catalyst concentration of 40 mM ammonia, some peaks inverted partially, including G2, T17, T3, T5 (the 5' end dimer thymine) and G9. T6, the other dimer residue remained positive at all mixing times. The inversion of residues in the sequence was varied, but with more catalyst concentration points, a more clear trend develops. All of the imino peaks follow the same trend in intensity with mixing time as observed in the parent spectra.

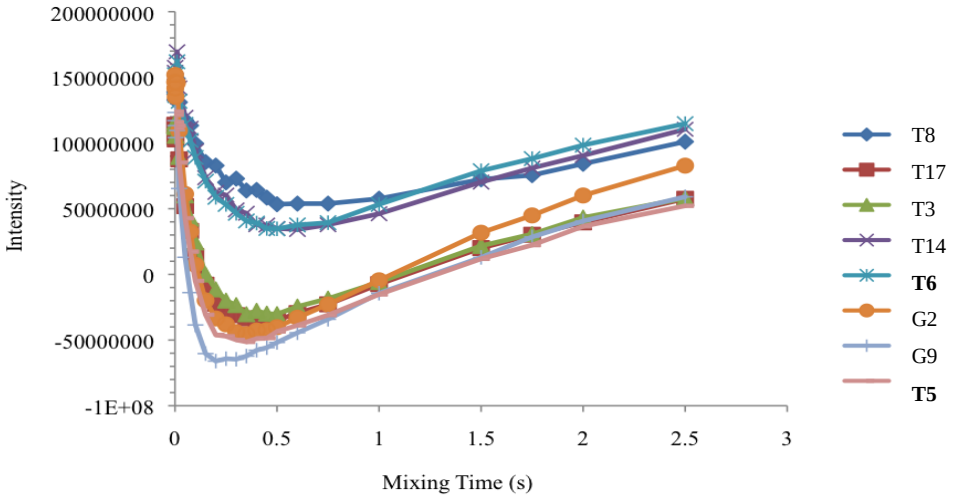

Figure 23. Individual imino protons of KK3TT4 in 40 mM ammonia catalyst. Peaks are labeled according to chemical shift. Noticeably, T5 has a negative intensity at a low range of mixing times, whereas T6 remains completely positive. We observed the residues of G2, T3, T17, T5 and G9 to have negative peaks.

We recorded 1Ds at ammonia catalyst concentrations of 40, 80, 100, 120 and 200 mM in KK34 and KK3TT4. (Figure 24) Although the peaks are not normalized in intensity to the phosphate buffer sample, the trend is clear. At 40 mM the peaks are well-resolved and indistinguishable from the phosphate buffer one-dimensional spectra taken previously (Figure 17). The end residues at 13.05 ppm are visible at this concentration. At 100 mM ammonia, there is significant shortening of the peaks, but little broadening. The penultimate guanine residues G2 and G9 observed at 12.7 ppm begin to shorten considerably, becoming very difficult to resolve. At catalyst concentrations higher than 40 mM, the end peaks are indistinguishable from the baseline. We noticed that the NMR tube was cracked at the top, and the solution volume was dropping due to evaporation. Since ammonia is a volatile chemical, we dialyzed the parent sample in 120 mM ammonia, and then recorded spectra for 120 mM and 200 mM. Unfortunately, the dialysis greatly diluted our sample, and as a result, the peaks for these titration points are shorter than expected. At 120 and 200 mM, all the peaks are uniformly broadened and shortened into the baseline. Since some very broad peaks are still observed at 200 mM, we have yet to hit the catalyst threshold of extremely fast exchange, and can still increase concentrations to 400 mM and 800 mM ammonia.

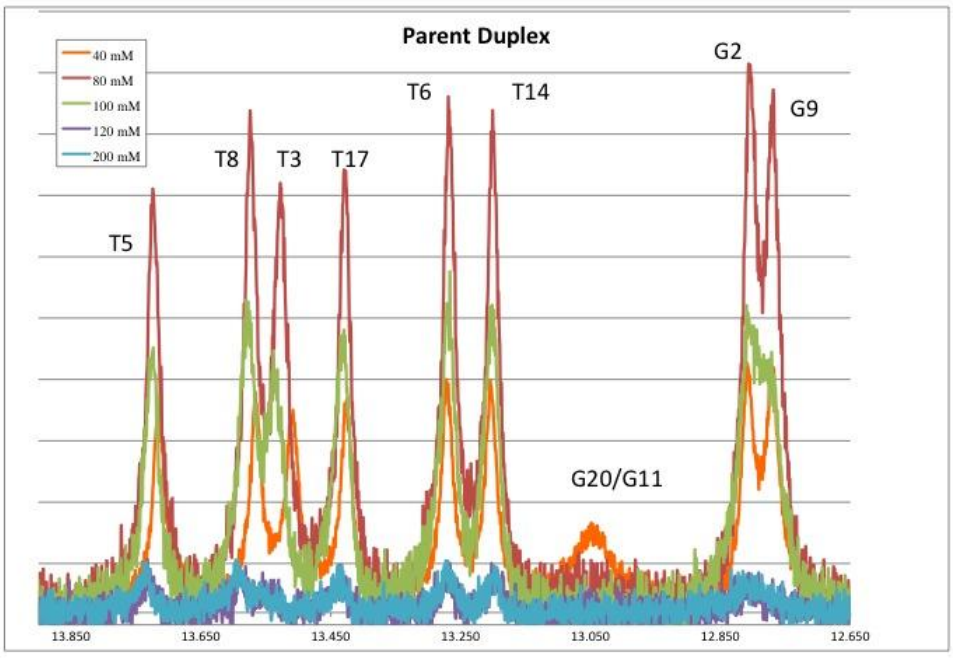

Figure 24. Overlaid imino regions of KK34 for five increasing catalyst concentrations. As catalyst concentration is increased, the peaks become uniformly shorter, with the exception of the 40 mM ammonia sample. The penultimate guanine residues are broadening, and the peak dispersion, especially at 12.7 ppm, is poor. At catalyst concentrations higher than 40 mM, the end peak at 13.05 ppm exchanges too fast to show a peak. At 200 mM, the peaks are all extremely short and broad, almost disappearing into the baseline.

Similarly, we overlaid a plot of the dimer sequence (Figure 25). For the dimer sample, we overlaid only four ammonia catalyst concentrations of 40, 80, 120 and 200 mM. Possibly due to cold denaturation of the sample, the 100 mM spectrum was poorly resolved and will be repeated. In comparison to the parent complex, the signal-to-noise ratio is much worse, with the baseline blurred, particularly in the 200 mM ammonia catalyst. The peaks at 40 mM ammonia are most intense, and follow a trend of decreasing in height with increased catalyst. The shortening and broadening trend of the peaks differs from the parent complex in significant residues. At 11.75 ppm, the 5' thymine dimer residue T5 shortens and broadens significantly from 40 mM ammonia to 80 mM ammonia, especially compared to the other peaks. At 120 and 200 mM, the T5 residue is very broad and begins to disappear into the noise of the baseline. Conversely, the 3' thymine dimer residue T6 at 12.75 ppm does not shorten and broaden in any significant or irregular way. Consistently, the penultimate guanines G2 and G9 at 12.6-12.4 ppm shorten and broaden quickly, at a slightly slower rate than T5. The peaks become so broad that they meld into a single peak. The nondescript mid-sequence T17 and T3 also broaden into a single peak.

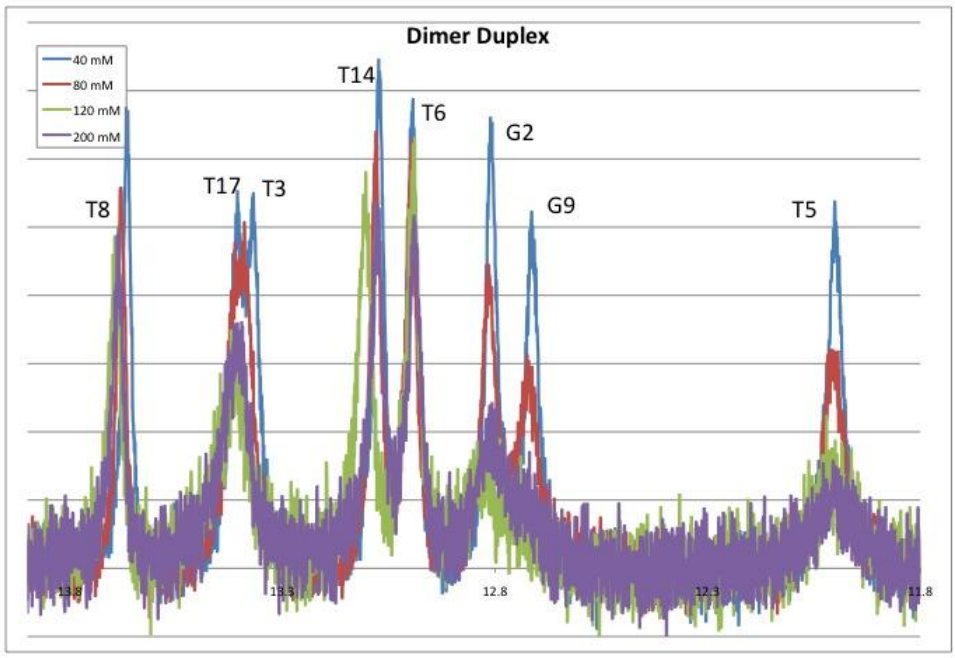

Figure 25. KK3TT4 imino region at four increasing ammonia catalyst concentrations of 40, 80, 120 and 200 mM. The 100 mM spectrum was poorly resolved and will be repeated. The signal-to-noise ratio is much worse compared to the parent, especially in the 200 mM sample (indicated in purple). The 5’ thymine dimer residue T5 at 11.75 ppm quickly shortens and broadens, compared to the other peaks. The penultimate guanines G2 and G9 at 12.6-12.4 ppm also shorten and broaden into one peak, as observed in the parent. T17 and T3 also broaden into a single peak. The 3’ thymine dimer residue T6 at 12.75 ppm does not appear to broaden.

Using Matlab, we fitted the peaks to find the exchange rate per residue at each concentration of ammonia catalyst (40, 80, 120 and 200 mM), for both the parent and dimer duplexes. By taking the inverse of exchange rate, we calculated the base pair lifetime, shown below (Table 7).

The exchange rates for each residue in the parent duplex were plotted against ammonia concentration at five points: 40, 80, 100, 120 and 200 mM (Figure 26). The trend of positive slopes indicates with increasing ammonia catalyst concentration, an increase in the rate of exchange is observed. As consistent with previous data, the penultimate end residues G2 and G9 show the greatest increase in exchange rate as catalyst concentration increases. The data is fit to a straight line consistent with equation 9. More catalyst concentration points will create a clearer trend.

Table 7. Exchange rates and base pair lifetimes.

		Parent KK34		Dimer KK3TT4	
#Peak	$[NH_3]$ M	k_{ex} ($M^{-1}s^{-1}$)	τ (ms)	k_{ex} ($M^{-1}s^{-1}$)	τ (ms)
G2	0.04	2.53	394.6	7.863	127.2
	0.08	3.52	284.3	22.138	45.17
	0.12	104.96	9.528	--	--
	0.2	219.31	4.560	76.06	13.15
T3	0.04	1.91	523.8	6.135	163.0
	0.08	2.76	361.9	16.63	60.13
	0.12	11.74	85.16	103.432	9.668
	0.2	49.33	20.27	9.806	102.0
T17	0.04	1.56	641.8	7.634	131.0
	0.08	1.61	620.7	17.675	56.57
	0.12	8.02	124.8	74.923	13.33
	0.2	12.02	83.18	44.244	22.60
T5	0.04	0.90	1107	10.23	97.75
	0.08	0.90	1109	26.549	37.67
	0.12	3.19	313.5	75.156	13.31
	0.2	3.71	269.4	94.075	10.63
T6	0.04	1.28	783.1	2.984	335.1
	0.08	1.31	764.5	5.362	186.5
	0.12	7.80	128.3	18.46	54.17
	0.2	10.00	99.99	12.984	77.02
T14	0.04	2.88	346.9	2.355	424.6
	0.08	1.43	700.8	5.866	170.5
	0.2	8.95	111.7	19.555	51.14
T8	0.04	0.72	1383	1.488	672.0
	0.08	1.07	939.0	3.77	265.3
	0.12	10.79	92.72	14.092	70.96
	0.2	22.90	43.68	10.381	96.33
G9	0.04	3.01	331.9	15.667	63.83
	0.08	5.54	180.6	41.075	24.35
	0.12	73.59	13.59	111.829	8.942
	0.2	106.58	9.383	179.98	5.556

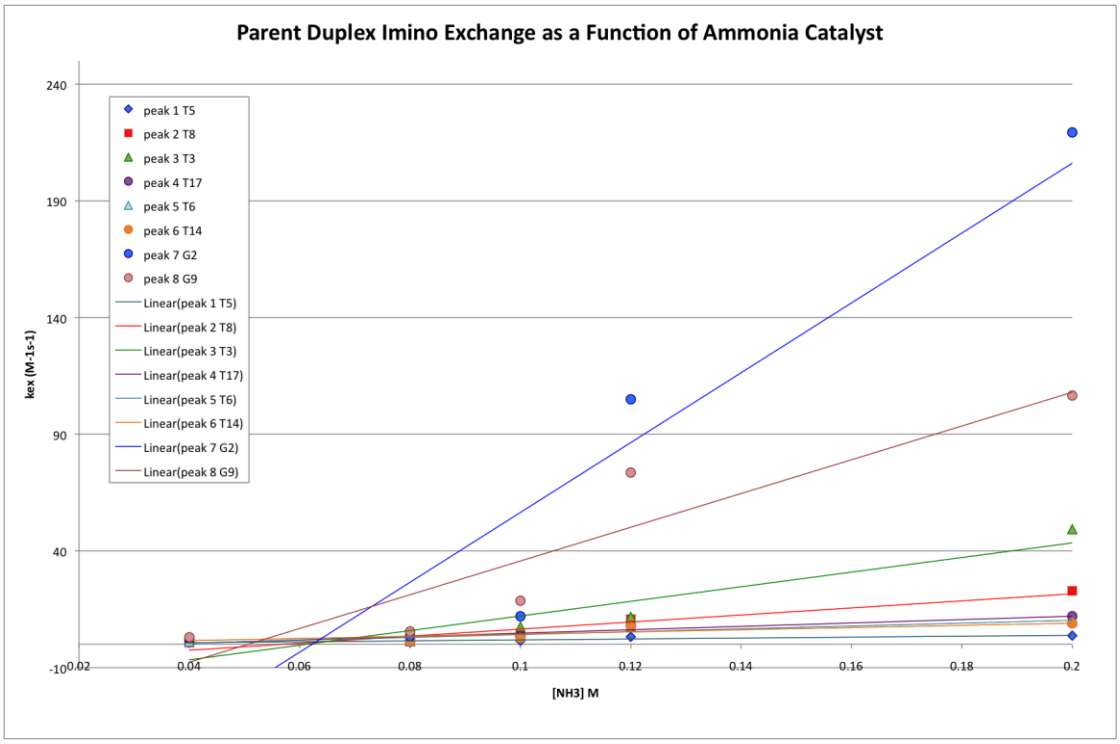

Figure 26. Exchange rates for each residue plotted against ammonia concentration for five points: 40, 80, 100, 120 and 200 mM. The positive slopes indicate that with increasing ammonia catalyst, there is an increase in the rate of exchange. The penultimate end residues G2 and G9 show the greatest increase in exchange rate.

In the dimer duplex (Figure 27) , the positive slopes indicate that increased exchange rate is proportional to increased catalyst concentration. The steepest slope corresponds to the most quickly increasing exchange rate. In the dimer sample, the G9 residue, a penultimate guanine residue, is the fastest-exchanging across all catalyst concentrations. Interestingly, the 5’ T5 dimer residue has a fast exchange for each catalyst concentration as well. The T5 residue has consistently fast exchange rates compared to the other residues. Pertinently, the 3’ T6 dimer residue has exchange rates similar to other thymines flanking the dimer, with no exceptional increase in exchange rate for these catalyst concentrations. The remaining thymine residues are clustered together at a relatively slow exchange rate.

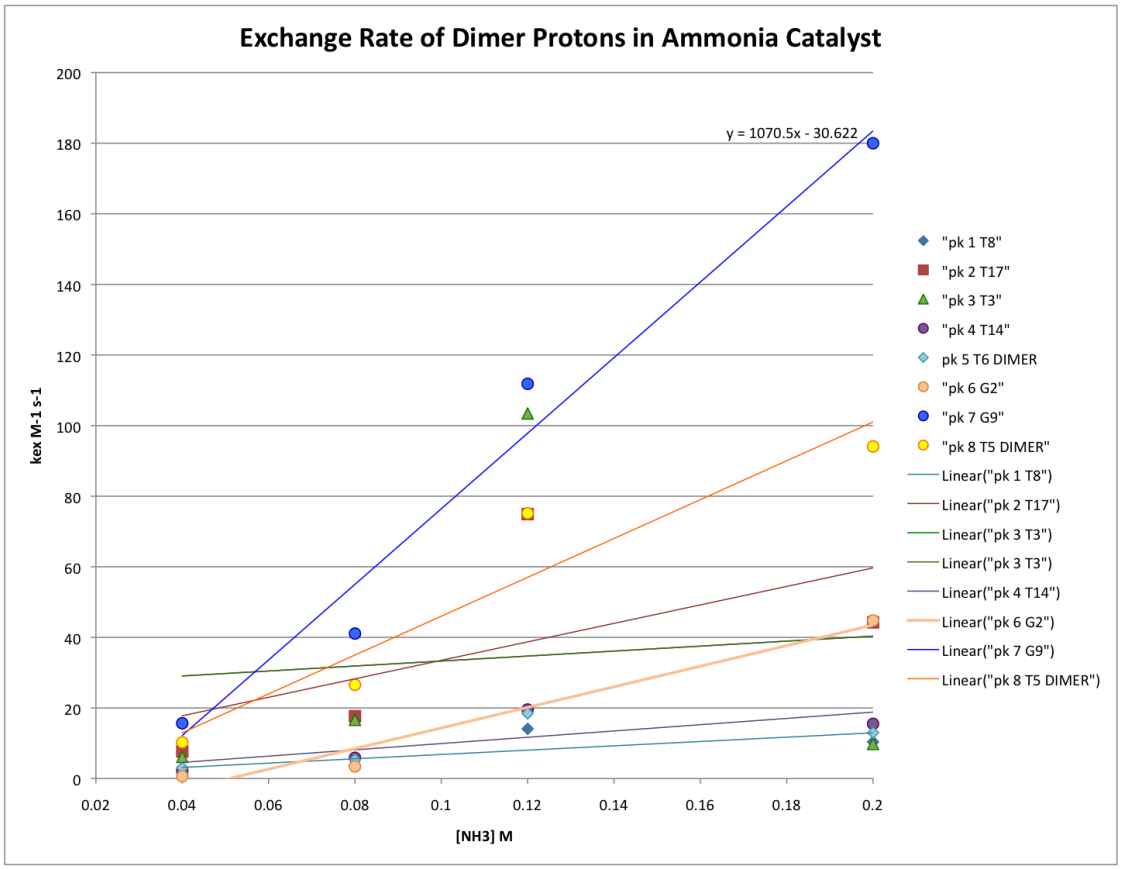

Figure 27. Plot of KK3TT4 exchange rate per residue as a function of ammonia catalyst concentration for four concentrations. The slope for each curve is positive, indicating increased exchange rate with increased catalyst concentration. The most quickly exchanging peak is the G9 residue, a penultimate guanine residue. The second-fastest exchanging residue is the 5' T5 dimer residue. The 3' T6 dimer residue is normal compared to the other residues.

The equilibrium constant of opening, K_{op} can be estimated from the slopes through the relationship

$$m = k_B * K_{op} \qquad (10)$$

using the k_B values for guanine and thymine respectively listed in section 3.1 These values are show in Table 8.

Table 8. Values for equilibrium constant of opening for each residue.

	Parent K_{op} ($M^{-1}s^{-1}$) $\times 10^{-6}$	Dimer K_{op} ($M^{-1}s^{-1}$) $\times 10^{-6}$
G2	2.0	0.81
T3	1.7	1.8
T17	0.40	6.9
T5	**0.11**	**1.4**
T6	0.34	1.8
T14	0.34	2.3
T8	0.84	1.8
G9	4.2	3.0

It is clear from Table 8 that the 5' dimer residue T5, T17, and T14 demonstrated the greatest increase in equilibrium constants of opening. The 3' dimer residue T6 shows a modest increase. T8 and T3 do not change significantly, and nor do the penultimate residues G2 and G9. The G2 and G9 residues are beginning to exchange so quickly in our experiments, that an accurate measurement for the rate constant is not currently available. The increase in the opening equilibrium constant of T5 is supportive of our theory that increased base pair opening is related to the destabiliziation of the duplex structure through the *cis-syn* thymine dimer lesion.

5. DISCUSSION

5.1. Sequence Selection

The 10 base pair oligonucleotide duplex KK34 and the 12 base pair duplex KK56 were compared for sequence optimization. The goal of the sequence design was to strike a balance between a small number of well-dispersed peaks, and a long-enough sequence to maintain the annealed structure in solution. A decamer was selected to form a complete turn of a B-DNA helix. A dodecamer was selected to encourage duplex formation even with the destabilizing lesion (*12).* The increase in sequence length adds stability to the duplex structure, contributing to reliably reproducible spectra. Enhanced peak dispersion could be accomplished by increasing magnet strength of the NMR instrument by moving up from a 400 MHz instrument to a 500 MHz, or by choosing a short sequence with fewer signals. In both KK34 and KK56, the lesion site was embedded in the center of the sequence, where the duplex is most stable. Considering the Brownian motion of the molecules in solution, we anticipated that the ends of the duplexes would fray spontaneously, so the exchange rates would be increased by the hidden variable of the duplex movement. The ends of both sequences are two C•G base pairs, to discourage fraying. C•G pairs are stronger than A•T pairs, because of an additional hydrogen bond.

Additionally, the dimer site was embedded in a length of unmodified DNA to examine the long-range effects of the lesion. A largely distorting lesion would be expected to change the overall structure of the duplex through

kinking the backbone as previous studies suggested (*14*). The kink would position residues that were previously farther than 6Å apart into close proximity, to change the NOE signals in the resultant NMR spectra. The dimer is flanked by alternating purine-pyrimidine residues to model an *in vivo* sequence where a *cis-syn* dimer would form after UV irradiation.

KK34 and KK56 were designed to be non-palindromic sequences, meaning the forward sequence is different than the reverse; when read from the 5' to 3', the sequence is unique compared to the 3' to 5'. A symmetric, palindromic sequence would be more thermodynamically stable in a single-stranded, homoduplex hairpin form, and the hairpin structure would be the predominant product during annealing, instead of forming a double-stranded helical structure.

5.2. NMR Resonance Assignment: Duplexes KK56 and KK5TT6

The full spectra of KK56 and KK5T6 correspond generally to the previously assigned double-stranded DNA spectrum (Figure 9). The thymine methyl protons are easily identified at 0.8 ppm by intense, clear signals. The sugar protons H2' and H3' are visible but not easily resolved at 2-3.5 ppm, and H4', H5' and H5'' appear at 4-4.5 ppm. The water peak at 4.7 ppm is suppressed, but obscures the sugar proton H3'. At the base of the large water peak, no ringing can be observed, which is identified by a sinusoidal undulation of the baseline that distorts the DNA peaks and occurs due to an imprecise suppression of water. In the deuterium oxide spectra, only the sugar and aromatic protons are visible, because we expect the deuterium to

exchange with the thymine and guanine imino and amino protons. In the water spectrum, amino peaks appear from cytosine, guanine and adenine at 6.5-8.5 ppm, flanking the aromatic ring protons at 7-8 ppm. The imino region is clear and far downfield at 11-13 ppm. The presence of the sugar, amino, and imino protons in the water spectrum indicates that the DNA was annealed and stable at the experimental temperature of 7°C. No unexplained peaks are present, which is indicative of a lack of impurities in our sample. Additionally, no spinning sidebands, which are tall peaks symmetrical about the water signal, are observed, which indicates good shimming and that the sample is homogenous in the magnetic field at the core of the NMR.

In the imino region of the parent KK56 in H_2O, nine distinct peaks are visible. Though we expect twelve peaks ideally, we would be content with ten peaks lacking the terminal base resonances. One missing peak suggests that one peak represents two residues, probably T7 and T9, because it appears significantly taller than the others. Since we would like to monitor the rate of exchange of each base pair individually, the overlap indicates that the sequence is not ideal. The two-dimensional spectrum allowed an unambiguous assignment of the imino region. The critical residue of T6, which will later be involved in the thymine dimer lesion, is isolated and well-resolved at 13.70 ppm.

In the dimer duplex KK5TT6, T6 shifts 1.61ppm to a position of 12.09 ppm, noticeably far upfield compared to all the other imino signals for the duplex. The shift, observed in previously published literature, is indicative of

the loss of aromaticity of T6 after the creation of the cyclobutane ring in the lesion. T7 migrates a shorter distance, but does shift 0.46 ppm upfield. In the parent spectrum, T6 is the furthest downfield peak, and in the dimer strand, T6 is the furthest upfield.

The duplex KK56 was rejected for the exchange experiments because of the poor peak dispersion and the overlap of peaks at the critical T7 residue. In the parent, T7 and T9 overlap, and in the dimer, T7 and G14 are overlaid. Ideally, T6 and T7 should be readily distinguishable from neighboring peaks. Deconvoluting and fitting overlapping peaks is a mathematically challenging task that becomes near-impossible as the peak heights begin to shorten and broaden as exchange catalyst is added.

5.3. NMR Resonance Assignment: Duplexes KK34 and KK3TT4

The full 1D spectrum of KK34 is very similar to the KK56 spectrum and to the general case of double-stranded DNA, exhibiting the same components (Figure 9). The presence of the sugar, amino, and imino protons in the water spectra indicate that the DNA was annealed in solution.

In the imino region, peaks for the KK34 sequence with and without the lesion showed good spectral resolution and allowed for mathematically straightforward peak fitting for the imino exchange experiments. None of the peaks are taller than the others, consistent with the equal concentrations of each kind of base pair, and every residue except the end peaks can be assigned. Eight peaks were observed, with two residues missing per end. This indicates that the critical T5 and T6 residues containing the dimer each have

its own distinct peak, which is the ideal case when we calculate an exchange rate for each imino of each residue. However, the peaks appear in a cluster, with overlap towards the baseline. Since the peak apexes can be distinguished, the overlap is not problematic. The sequence could be solved in a straightforward and unambiguous manner through the standard NOE sequential assignment. Though most of the residues in this duplex sequence have been assigned by Taylor *et al*., the imino peaks were not assigned (*12*). In our experiments, the imino region has been completely assigned, without gaps, from G2 to G9, excluding the terminal imino protons. In the parent duplex, the 5' end thymine dimer T5 is resolved at 13.44 ppm, and in the dimer complex, there is an obvious upfield shift to 11.78 ppm, as seen previously in the KK56/KK5TT6 duplex comparison. The 3' end thymine dimer T6 is originally resolved at 13.02ppm in the parent, but it also shifts upfield to 12.77 ppm. As expected, T5 has a more severe shift, due to the weakening of the hydrogen bonding interactions at the 5' end of the lesion. Taylor *et al*. suggest that the significant upfield shift (1.66 ppm) of the 5' T5 is due to ring current effects (*12*). The 3' end T6 has a less severe shift of 0.25ppm, since the hydrogen bond on the 3' side is less effected and remains close to normal.

Within the duplex structure, the chemical shifts of each residue are only significant for the 5' thymine (T5, in the case of KK34), as shown in Figure 28.

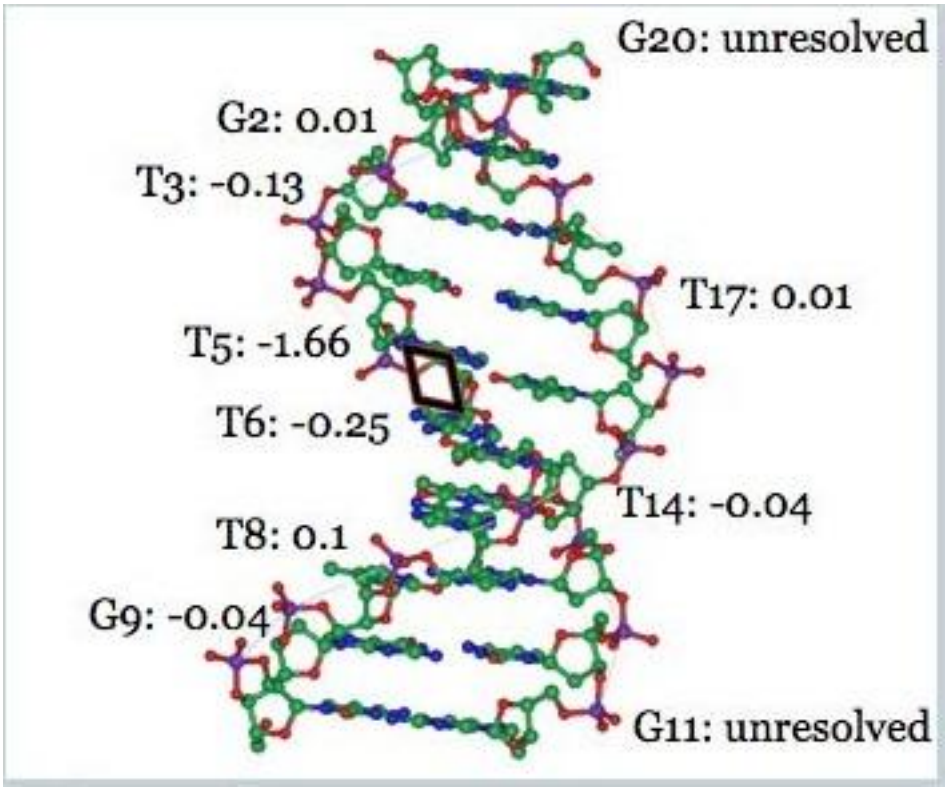

Figure 28. Chemical shift changes in the KK34 to KK3TT4 duplex. The black parallelogram represents the approximate position of the thymine dimer lesion, created with Nucleic Acid Builder.

We noticed the most radical change for T5, then for T6. The residues immediately flanking the dimer are also slightly perturbed, with the magnitude of the perturbations decreasing exponentially with distance from the lesion site. The chemical shifts of residues G2 and T3 upstream of the dimer, on the 5' side, have almost no chemical shift change (0.01 ppm change). The residues T6-G20 on the 3' side have more noticeable changes (up to 0.1 in the case of T8). The pattern of the shift change indicates that the lesion creates a downstream distortion, affecting the duplex structure towards the 3' side. These observations verify the suggestions made by Taylor on the KK34 sequence. Since Taylor *et al*. did not completely assign the imino region, the detrimental effect of the dimer on the 3' end was speculative. (*12)* Taylor *et al.* proposed crystal structures indicating that the *cis-syn* dimer has the 5' thymine of the dimer in the *anti* orientation, mimicking a normal conformation of a regular B-form thymine. Their group speculated that the lesion is not radically destabilizing from their model, and our NMR experiments suggest that the lesion is not extremely destabilizing (with disturbances below 2 ppm shifts), but there is a definitive destabilizing effect of the lesion within the duplex. From our work, we observe that the magnitude of the destabilization decreases with distance from the lesion, with a greater disturbance indicated on the 3' end.

The specific upfield shifting of T5, the 5' thymine, is indicative of the loss of aromaticity with the cyclobutane bond formation fusing the adjacent thymines. The change in the chemical environment of T5 is suggestive of a

change in the electronic structure of the dimer, since the π-stacking through the bases is interrupted. Additionally, nine rotatable bonds are made static in upon creation of the dimer: the two glycosyl bonds, the two sugar rings, and the five inter-nucleotide bonds. (*12*) In his paper, Taylor suggests the electronic structural change is due to ring current effects.

We decided to proceed with the exchange experiments using the 10-mer KK34 duplex. The peaks for the sequence with and without the lesion showed good spectral resolution and allowed for mathematically straightforward peak fitting for the imino exchange experiments because each residue on the duplex could be assigned to a well-resolved peak. The resolution of each peak allows for rate constants to be calculated for each guanine or thymine.

5.4. Exchange Experiments

The exchange experiments were designed to elucidate the rate of base pair opening using a series of one-dimensional ^{1}H NMR spectra of the imino region of the parent and dimer duplex in ammonia catalyst. 1D spectra are obtained at a range of mixing times to monitor how the height of each imino proton changes over time. The peak heights are integrated and the volumes are plotted at each mixing time.

To determine the rate of base pair opening, one-dimensional ^{1}H NMR spectra are taken at a range of mixing times. By graphically stacking the 24 different spectra at 24 different mixing times, we can observe the sample is functioning as expected in the NMR, and the peak heights change in intensity

with mixing time. (Figure 20, 21) Our model predicts that the bases open to the solvent, and the imino protons exchange with the water protons with a rate k_{ex}. As the water protons are pulsed, they invert and recover, along with the imino protons, with rates of Rl_w and Rl_i respectively. A minimum height is observed at 0.5 ms.

In the parent sequence at 40 mM, T3, G2 and G9 have the fastest exchange rates, indicated by the significant dip in peak intensity on the volume versus mixing time plot. These residues are closest to the ends, and are expected to be exposed more often to the solvent since the residues on the ends are frayed and are completely open to solvent exchange. The residues at the center of the complex, such as T5 and T6, have the slowest exchange rates, indicated by the shallowest slopes at any given point on the exchange curve. (Figure 22, 23) Neither T5 nor T6 show a dramatic decrease in peak height, and remain at a fairly high peak intensity throughout the exchange experiment (0-3 s mixing time).

In the dimer duplex, the residues of G2, T3, T17, T5 and G9 are observed to have fast exchange. The penultimate residues of G2 and G9, and the antepenultimate residue T3 remain residues of fast exchange from the parent to the dimer. Interestingly, we observed that T17 and T5 have fast exchange in the dimer. As the 5' thymine dimer residue, the T5 residue complies with our hypothesis that the lesion presence augments exchange rate. Notably, the 3' end residue, T6, does not share the fast exchange. It is possible that at higher catalyst concentrations T6 will join T5 in fast exchange.

Interestingly, we observed that T17 has a very vast exchange in the dimer. T17 is the 5' neighbor of T5, and this result indicates that the exchange rate perturbation is more significant upstream of the dimer. This adds an interesting insight on the kinetics of the duplex, considering the one-dimensional NMR chemical shift changes indicated that the region of greatest chemical change was to the 3' end.

It is known that AT and GC base pairs have different opening lifetimes; adjacent AT pairs exchange with a lifetime of ~ 0 to 50 ms, whereas adjacent GC pairs stay closed longer, on the order of from 50 to 350 ms. (*26*) The lifetimes are sequence dependent, and another group has reported values of 10-50 ms for G-C pairs, and 1-5 ms for A-T pairs. (*17*) Previous research has indicated that in increasing ammonia catalyst concentration, the exchange rate is not limited by individual base-pair dynamics. At infinite catalyst concentration, the exchange rate is reflecting the entire duplex movement of exchange. Conversely, at the lowest or zero catalyst concentration, the rate constant can be expected to be the largest.

From the exchange rate data, we calculated the base pair lifetime per residue for 40, 80, 120, and 200 mM ammonia. The expected lifetime for a cytosine-guanine pair is 10-50 ms, and an adenine-thymine pair is 1-5 ms (*17*). In the parent duplex at 40 mM ammonia, we are far from this range; our values for lifetime of T5 is 642 ms, and for G2 it is 394 ms. At the next titration point of 80 mM, we observe a shortening of the lifetime; for T5 dropped to 620 ms and G2 dropped to 284 ms. Still, compared to the literature

values, we are far away from the catalyst concentration to observe those lifetimes. At our highest concentration of 200 mM, T5 is at 269 ms. However, we are trending in the correct direction, and larger steps in ammonia catalyst concentration will help us approach the ideal concentration, in which one exchange per opening event can be assumed. The effect is more drastic in the dimer sequence; in 40 mM, G2 has a much lower lifetime than the parent, at 127 ms. Comparatively, T5 has a lifetime of 97 ms in 40 mM ammonia. At our highest concentration, T5 is approaching the correct range with 22 ms opening, and G2 has fallen within the range, at 13 ms.

Thus, we plan to add more ammonia catalyst, up to a concentration of 1 M, if possible. Currently, our data reflects the ammonia concentrations of 40, 80, 100, 120 and 200 mM total ammonia. It is important to consider that even with achieving a high concentration, such that we can model one exchange event per opening, we do not know the mechanism of base flipping initiation. It is possible that exchange can occur from the thymine flipping out, and it is equally possible that the opposite adenine opens, allowing for exchange.

The rates of base pair opening and closing (k_{op} and k_{cl},) could not be found using Equation 7 with only four data points. However, K_{op} could be approximated by a linear fit to a plot of exchange rate (k_{ex}) versus catalyst concentration [B] as described by equation 9 (Figures 26, 27). In the parent complex, the 5' thymine dimer residue T5 had an equilibrium constant of opening of $0.11 \times 10^{-6}\ M^{-1}s^{-1}$ in the parent complex, and increased to 1.4×10^{-6}

$M^{-1}s^{-1}$ in the dimer form. Significant increases in equilibrium constants of opening were also observed for dimer-flanking residues T14 and T17. T6 had a modest increase in K_{op}, but interestingly less than that of T14 and T17. The exciting result of the increase in equilibrium opening constant for T5 indicates that there is a thermodynamic and probably also kinetic effect of the dimer that allows rapid, frequent exchange of the imino proton. Our data supports the suggestion that the *cis-syn* cyclobutane thymine dimer destabilizes the DNA duplex enough, leading to base opening to the solvent at an augmented rate.

5.5. Relation to Homologous Research

Insight into the mechanism of thymine base flipping has been gained previously using uracil. The repair mechanism of uracil DNA glycosylase (UDG), the repair enzyme for unwanted uracil bases, was modified to be catalytically active against thymine after selective amino acid replacement. (*27*) Imino proton exchange experiments were performed on the UDG and uracil containing-DNA. Cao *et al.* found that the binding of the enzyme UDG accelerates the imino proton exchange of thymine; the thymine resonance being excised was found to have an exchange 25-fold faster compared to that in the free DNA. In comparison, the thymine imino resonance near the end of the DNA sequence showed a five-fold increase in exchange rate after binding. Pertinently, the UDG was found to have no effect on the imino proton exchange of guanine, suggesting that the enzyme uses the flexibility of the AT basepair (containing only two hydrogen bonds), compared to the more rigid

CG basepair (containing three hydrogen bonds). The excised guanine resonance was observed to have a four-fold increase in exchange rate, which can be explained by local perturbation of the duplex when UDG binds. UDG preferentially opened the AT pair, because of the fewer number of hydrogen bonds. In the exchange experiments, the exchange rate was dependent strongly on catalyst concentration and could be fit to find the rate constants for base pair opening and closing, as well as the equilibrium constant for base pair opening ($\alpha K_{op} = k_{op} / k_{cl}$). The authors found that UDG increases the opening equilibrium for the excised thymine base by 75- to 280-fold. Comparatively, the excised guanine only observed a 2-fold increase. The enzyme itself is likely to be stabilizing the DNA duplex, maintaining the open, solvent-exposed state of the excised bases. The authors concluded that the repair enzyme traps the open state of the AT basepair, without significantly altering the rate of base pair opening. The enzyme increases the αK_{op} term by reducing the rate of closing (k_{cl}). Concerning uracil, the group found that the enzyme advantageously used the instability of uracil to initiate the spontaneous flipping out of the duplex, generating a high-energy intermediate. UDG can then weakly interact with the DNA backbone, trapping the high-energy uracil, and cleave at the glycosidic bond. Using equation 3, the authors Cao *et al.* plotted inverse exchange rate ($1/k_{ex}$) versus inverse catalyst concentration (1/[B]), to generate a curve that described the relative magnitude of catalyst exchange $k_B[B]$ and rate of internal catalysis k_{int}. (*27*)

In a follow-up study on UDG, the stabilization of the open complex was shown to flatten the energy landscape for base flipping. In this way, the thymine being excised can be rotated away from the base stack in a series of energetically downhill steps. (*28*)

In our system of a dimer-repairing enzyme, a similar mechanism could be acting. The increased opening at the thymine dimer site could be helpful to an enzyme that must rotate out the dimer, while stabilizing the opposite strand. The cyclobutane ring involved in the dimer is a particularly rigid structure, and the locked conformation could be useful to an enzyme involved in repair.

6. CONCLUSION

The results from the one-dimensional NMR comparisons of the parent and dimer duplexes indicated significant changes in the chemical environments of the protons, correlating to a destabilizing effect of the dimer lesion. In KK56/KK5TT6, we observed the thymines associated with the dimer (T6 and T7) to exhibit noticeable shifts in frequency from the parent to the dimer. In the 10-mer duplex KK34/KK3TT4, a similar shifting effect was observed, but every residue (including dimer residues T5 and T6) is well resolved in both parent and dimer structures. We used the 10-mer sequence to consider the kinetic destabilization through the imino exchange experiments. The perturbations in chemical shift were more significant downstream of the dimer, on the 3' end, compared to the 5' end.

From the exchange experiments, the 5' thymine dimer residue T5 had an equilibrium constant of opening K_{op} of $0.11 \times 10^{-6}\ M^{-1}s^{-1}$ in the parent complex, and increased to $1.4 \times 10^{-6}\ M^{-1}s^{-1}$ in the dimer form. The base pair lifetime calculations indicate that we are not at the ideal catalyst concentration to model one exchange event per opening. The increase in equilibrium opening constant for T5 suggests that there is a kinetic effect of the dimer that allows rapid, frequent exchange of the imino proton involved in the hydrogen bonding between strands. Our data support the suggestion that the *cis-syn* cyclobutane thymine dimer destabilizes the DNA duplex enough to allow base opening to the solvent at an augmented rate.

7. REFERENCES

(*1*) Friedberg, E.C. (1997) *Correcting the Blueprint of Life: a Historical Account of the Discovery of DNA Repair Mechanisms*. Cold Spring Harbor Laboratory Press, Cold Spring Harbor, N.Y.

(*2*) Friedberg, E. C.; Walker, G.C.; Siede, W.; Wood, R.D.; Schultz, R.A.; Ellenberger, T. (2006) *DNA Repair and Mutagenesis*. ASM Press, Washington, DC. 2nd Ed.

(*3*) Watson, J.D. and Crick, F.H.C. (1953) Molecular structure of nucleic acids. *Nature.* **171**: 737-738.

(*4*) Lodish, H.; Berk, A.; Kaiser, C. A.; Krieger, M.; Scott, M. P.; Bretscher, A.; Ploegh, H. (2008). *Molecular Cell Biology*. Macmillan, New York, NY. 5th Ed.

(*5*) Nelson, D.L.; Lehninger, A.L.; Cox, M.M.; Freeman, W.H. (2008) *Lehninger Principles of Biochemistry*. Freeman Publishing. 5th Ed.

(*6*) Cheng, K.C.; Cahill, D.S.; Kasai, H.; Nishimura, S.; Loeb, L.A. (1992) 8-Hydroxyguanine, an abundant form of oxidative damage, causes G → T and A→ C substitutions. *J. Biol. Chem.* **33**: 166-171.

(*7*) Li, J.; Uchida, T.; Todo, T.; Kitagawa, T. (2006) Similarities and differences between cyclobutane pyrimidine photolyase and (6-4) photolyase as revealed by resonance Raman spectroscopy. *J. Biol. Chem.* **281**: 25551-25559.

(*8*) Douki, T.; Laporte, G.; Cadet, J. (2003) Inter-strand photoproducts are produced in high yield within A-DNA exposed to UVC radiation. *Nucl. Acids Res.* **31**: 3134-3142

(*9*) Mitchell , D.L.; Jen, J.; Cleaver, J.E. (1992) Sequence specificity of cyclobutane pyrimidine dimers in DNA treated with solar (ultraviolet B) radiation. *Nucl. Acid. Res.* **20**: 225-229.

(*10*) Radany, E.H.; Love, J.D.; Friedberg, E.C. (1981) The use of direct photoreversal of UV-irradiated DNA for the demonstration of pyrimidine dimer-DNA glycosylase activity, *Chromosome Damage and Repair*. Plenum Publishing Corp, New York, NY.

(*11*) Frankel. E.F.; (2011) *Thermodynamic Effects of the* cis-syn *Thymine Dimer Lesion on Duplex DNA.* Mount Holyoke College Senior Symposium. April 2011.

(*12*) Taylor, J.S.; Garrett, D.S.; Brockie, I.R.; Svoboda, D.L.; Tesler, J. (1990) ^{1}H NMR Assignment and Melting Temperature Study of *cis-syn* and *trans-syn* Thymine Dimer Containing Duplexes of d(CGTATTATGC)· d(GCATAATACG). *Biochemistry* **29**, 8858-8866.

(*13*) Johnson, R.E.; Prakash, S.; Prakash, L. (1999) Efficient bypass of a thymine-thymine dimer by yeast DNA polymerase, pol eta. *Science* **283**. 1001-1004.

(*14*) Park, H.; Zhang, K.; Ren, Y.; Nadji, S.; Sinha, N.; Taylor, J.S.; Kang, C. (2002) Crystal structure of a DNA decamer containing a *cis-syn* thymine dimer. *Proc. Natl. Acad. Sci. USA* **99**. 15965-15970.

(*15*) Kim, J.K.; Patel, D.; Choi, B.S. (1995) Contrasting structural impacts induced by *cis-syn* cyclobutane dimer and (6-4) adduct in DNA duplex decamers: implication in mutagenesis and repair activity. *Photochem. Photobiol.* **62**: 44-50.

(*16*) Sancar, A. (2008) Photolyase and *in vivo* enzymology: 50th anniversary. *Biol. Chem.* **283**: 32153-32157.

(*17*) Priyakumar, U.D. and MacKerell, A.D. (2006) NMR imino proton exchange experiments on duplex DNA primarily monitor the opening of purine bases. *J. Am. Chem. Soc.* **128**: 678-679.

(*18*) Guéron, M.; Kochoyan, M,; Leroy JL. (1987) A single mode of DNA base-pair opening drives imino proton exchange. *Nature.* **328**: 89-92.

(*19*) Warmlander, S.; Sen, A.; Leijon, M. (2000) Imino proton exchange in DNA catalyzed by ammonia and trimethylamine: evidence for a secondary long-lived open state of the base pair. *Biochemistry.* **39**: 607-615.

(20*)* Bishop, K.D. (2011) Structure Determination by NMR. www.nmr2.buffalo.edu/resources/edu/matr/structure-determination.ppt. Accessed March, 2011.

(*21*) James, T.L. (2001) NMR Determination of Oligonucleotide Structure. *Curr. Prot. Nucl. Acid Chem.* **7.2.1.-7.2.16.**

(*22*) Fawzi N.L.; Phillips A.H.; Ruscio J.Z.; Doucleff M.; Wemmer D.E.; Head-Gordon T. (2008) Structure and dynamics of the Abeta(21-30) peptide

from the interplay of NMR experiments and molecular simulations. *J. Am. Chem. Soc.* **130**: 6145-58.

(*23*) Folta-Stogniew, E. and Russu, I. (1996) Base-catalysis of imino proton exchange in DNA: effects of catalyst upon DNA structure and dynamics. *Biochem.* **25**. 8439-8449.

(*24*) Plateau, P.; Guéron, M. (1982) Exchangeable proton NMR without base-line distortions, using new strong-pulse sequences, *J. Am. Chem. Soc.* **104**: 7310–7311.

(*25*) Chen, C.; Cohen, J.; Behe, M. (1983) B to Z Transition of Double-Stranded Poly[deoxyguanylyl(3'-5')-5-methyldeoxycytidine] in Solution by Phosphorus-31 and Carbon -13 Nuclear Magnetic Resonance Spectroscopy. *Biochemistry.* **22:** 2136-2142.

(*26*) Dhavan, G.M.; Lapham, J.; Shuwei, Y.; Crothers, D.M. (1999) Decreased imino proton exchange and base-pair opening in the IHF-DNA complex measured by NMR. *J. Mol. Biol.* **288**: 659-671.

(*27*) Cao, C.; Jiang, Y. L.; Stivers, J.T.; Song, F. (2004) Dynamic opening of DNA during the enzymatic search for a damaged base. *Nat. Struc. Molec. Biol*. **11**: 1230-1236.

(*28*) Parker, J.B.; Bianchet, M.A.; Krosky, D.J.; Friedman, J. I.; Amzel, L.M.; Stivers, J.T. (2007) Enzymatic capture of an extrahelical thymine in search for uracil in DNA. *Nature.* **449**: 433-437.